

國立交通大學

光電工程研究所

碩士論文

新型低溫配向膜材料研究

**New Liquid Crystal Alignment Materials for
Low Temperature Process**

研究生：林秀玉

指導教授：陳皇銘 博士

指導教授：許瑤真 博士

中華民國九十九年七月

新型低溫配向膜材料研究

New Liquid Crystal Alignment Materials for Low Temperature Process

研究生：林秀玉

Student : Xiu-Yu Lin

指導教授：陳皇銘 博士

Advisor : Dr. Huang-Ming Philip Chen

許瑤真 博士

Advisor : Dr. Yao-Jane Hsu

國立交通大學



Submitted to Institute of Electro-Optical Engineering

College of Electrical and Computer Engineering

National Chiao Tung University

in Partial Fulfillment of the Requirements

for the Degree of Master

in

Electro-Optical Engineering

July 2010

Hsinchu, Taiwan, Republic of China

中華民國九十九年七月

新型低溫配向膜材料研究

學生：林 秀 玉

指導教授：陳皇銘

指導教授：許瑤真

國立交通大學光電工程研究所



液晶配向層材料在影像品質以及液晶顯示可靠度扮演重要的角色。對聚亞醯胺層(Polyimide film)的配向摩擦(Rubbing)方法會影響配向膜的製備。然而，製備此配向膜的烘烤溫度高於 200°C 是使其在軟性基板應用上的主要限制因素。此外，可用於低溫製程之新型液晶配向材料為節能的新興需求。因此，各種具有明顯的化學官能基例如聚乙烯醇(polyvinyl alcohol, PVA)、聚苯乙烯(polystyrene, PS)、聚苯乙烯磺酸(polystyrene sulfonic acid, PSSA)、聚(4-乙基苯酚)(poly(4-vinylphenol, PVP)和聚乙吡咯烷酮(polyvinyl pyrrolidone, PVPD)皆列入研究材料中。這些材料的製程溫度都可以低於 110°C 。

我們研究了各種高分子表面在作為液晶顯示器上之新型液晶配向材料的光學特性和表面定向。並檢驗這些新型液晶配向材料在機械摩擦配向處理後的光電特性、指向秩序參數(order parameter)和極化錨定能(polar anchoring energy)等等表現。這些新型液晶配向材料的鍵結定向可以透過表面選擇性技術，即近緣 X-射線

吸收細微組態(near edge X-ray absorption fine structure, NEXAFS)來作歸類。NEXAFS 的測量結果明顯地顯示配向摩擦後的高分子表面面內和面外的不對稱性。可證實這些新型液晶配向材料是適合用於平板液晶顯示器低溫製程的軟性基板上。



New Liquid Crystal Alignment Materials for Low Temperature Process

Student: Lam Tu Ngoc
(Xiu-Yu Lin)

Advisor: Dr. Huang-Ming Philip Chen
Advisor: Dr. Yao-Jane Hsu

Institute of Electro-Optical Engineering
National Chiao Tung University

Abstract

Liquid crystal alignment layer plays an important role to the image quality and liquid crystal display's reliability. The rubbing method on polyimide (PI) film has dominated the alignment films' preparation. However, high baking temperature over 200⁰C that is required for the film preparation is a major limitation for its applications into flexible substrates. New alignment materials for low temperature process are the emerging needs of energy conservation. Various alignment materials containing distinct chemical functional groups, such as polyvinyl alcohol (PVA), polystyrene (PS), polystyrene sulfonic acid (PSSA), poly-(4-vinylphenol) (PVP) and polyvinylpyrrolidone (PVPD) are studied. The process temperature for these materials can be as low as 110⁰C.

Optical properties and surface orientation of a variety of polymer surfaces were investigated as new liquid crystal alignment materials in liquid crystal displays (LCDs). The performances of these new liquid crystal alignment materials induced by mechanical rubbing treatment were examined by their electro-optical properties, order parameter and polar anchoring energy. The bonding orientation of these new alignment materials were characterized through surface sensitive technique, near edge

X-ray absorption fine structure (NEXAFS). The NEXAFS measurements clearly indicated the in plane and out of plane asymmetries at the surface of rubbed polymers. These new liquid crystal alignment layers are suitable for flexible substrates of low temperature process in flat panel liquid crystal displays.



Acknowledgement

The completion of this thesis could not be done without the help and support of many people who are gratefully acknowledged. I was lucky enough to receive this kind of aid from many sources.

First of all, I am honored to express my deepest gratitude to my advisors, Prof. Huang-Ming Philip Chen and Dr. Yao-Jane Hsu who have helped me a lot in finishing this thesis. I greatly appreciate their kindness. They not only have offered precious ideas, advices, and suggestions but also have encouraged and motivated me try my best to reach my target.

Secondly, I am really thankful to the professors who taught me useful and interesting courses at National Chiao Tung University as well as at National Synchrotron Radiation Research Center.



Thirdly, I am indebted to many of my friends to support me during the master program. I highly appreciate all the input that I have received from my classmates. I especially owe sincere thanks to my good friends in NSRRC, who have helped and encouraged me very much during the whole time. Friendships will be with me wherever I go. I have learned a lot from everyone that I worked with. I will try to acquire valuable knowledge from my teachers and classmates to enrich my life.

Last but not least, I would like to thank my family for their support all the way from the beginning of my study.

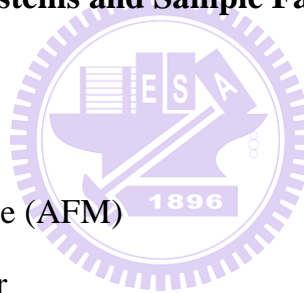
Thank you very much for all your kind help and guidance.

Table of contents

Abstract in Chinese	i
Abstract in English	iii
Acknowledgement	v
Table of contents	vi
List of Tables	ix
List of Figures	x
Chapter 1 Introduction	1
1.1 Display Technology	1
1.2 Introduction of Liquid Crystal	1
1.3 Liquid Crystal Displays	3
1.3.1 The Fundamental Concept of Liquid Crystal Displays	3
1.3.2 Operation Principle of Twisted Nematic Liquid Crystal	7
1.4 Liquid Crystal Alignment	8
1.4.1 Alignment Techniques	8
1.4.2 Alignment Materials	9
1.5 Motivation and Objective	9
1.6 Organization of This Thesis	11



Chapter 2	Principle of Liquid Crystal Alignment and Near Edge X-ray Absorption Fine Structure (NEXAFS) Spectroscopy	12
2.1	Mechanical Rubbing Technique	12
2.1.1	Rubbing Strength	12
2.1.2	Alignment Mechanism Induced by Rubbing Method	14
2.2	Near Edge X-ray Absorption Fine Structure (NEXAFS) Spectroscopy	19
2.2.1	Elliptically Polarized Undulator (EPU)	19
2.2.2	Photoemission Electron Microscopic (PEEM)	20
2.2.3	The Operation Principle of NEXAFS Spectroscopy	21
Chapter 3	Measurement Systems and Sample Fabrication	26
3.1	Introduction	26
3.2	Atomic Force Microscope (AFM)	26
3.3	UV-Visible Spectrometer	28
3.3.1	Cell Gap Measurement	28
3.3.2	Order Parameter Measurement	31
3.4	Electro-Optical Measurement System	31
3.5	Anchoring Energy Measurement	32
3.6	NEXAFS Measurement	35
3.7	Fabrication Process	36
3.7.1	Flowchart	36
3.7.2	Fabrication Process	37



Chapter 4	Experimental Results and Discussion	40
4.1	Surface Morphology of Alignment Materials	40
4.2	Order Parameter	44
4.3	Electro-optical Characteristics of TN cells	45
4.4	Polar Anchoring Energy	47
4.5	NEXAFS Measurements	58
Chapter 5	Conclusions	64
5.1	Conclusions	64
5.2	Future Works	66
References		67



List of Tables

- Table 2-1** Alignment obtained with various rubbed polymer films
- Table 3-1** Specific parameters of spin coating process for solvent (top) and mixture solution (bottom)
- Table 3-2** Specific parameters of different materials
- Table 4-1** Chemical structures of different materials
- Table 4-2** Order parameters of different rubbed polymers
- Table 4-3** Specific parameters of V-T curves using different rubbed surfaces
- Table 4.4** Rubbing parameters at three different rubbing conditions
- Table 4-5** Necessary parameters for determining polar anchoring energy of polyimide at different rubbing strength conditions
- Table 4-6** Necessary parameters for determining polar anchoring energy of PSSA at different rubbing strength conditions
- Table 4-7** Necessary parameters for determining polar anchoring energy of PVP at different rubbing strength conditions
- Table 4-8** Order parameters of rubbed PI, PSSA, and PVP at strong rubbing strength
- Table 4-9** Necessary parameters for determining polar anchoring energy of PVPD at different rubbing strength conditions

List of Figures

- Fig. 1-1** Schematic illustration of crystal, liquid crystal, and liquid phases
- Fig. 1-2** Device structure of transmissive LCD
- Fig. 1-3** (a) Sketch of Transmissive LCD, (b) Reflective LCD, and (c) Transflective LCD
- Fig. 1-4** The operation principle of normally white twisted nematic LCD
- Fig. 1-5** Typical orientations of nematic liquid crystals on alignment layer
- Fig. 2-1** Photograph of rubbing machine
- Fig. 2-2** Schematic of mechanical rubbing
- Fig. 2-3** The geometry of shear deformation in cross section
- Fig. 2-4** Plot of retardation induced by rubbing
- Fig. 2-5** Liquid crystal orientation on rubbed surfaces
- Fig. 2-6** NEXAFS spectra recorded by Auger (AEY) and total (TEY) electron yield for rubbed BPDA-PDA polyimide (in the left) and rubbed 96K polystyrene (in the right), with the electric field parallel to x, y and 20° from the z axis
- Fig. 2-7** The formation of linearly polarized light by EPU
- Fig. 2-8** Experimental photon flux spectrum of the EPU beamline
- Fig. 2-9** PEEM station at EPU
- Fig. 2-10** Illustration of absorption region of XANEX and EXAFS
- Fig. 2-11** NEXAFS spectrum of different elements in a polyimide polymer
- Fig. 2-12** Near edge X-ray absorption fine structure spectrum (Carbon K-edge)
- Fig. 2-13** Polarization dependent NEXAFS spectra of benzene chemisorbed on Ag (110)
- Fig. 2-14** Two techniques to record X-ray absorption spectra
- Fig. 2-15** Schematic diagram of a diatomic molecule

- Fig. 3-1** Concept of AFM and the optical lever
- Fig. 3-2** Two reflecting surfaces separated by a layer causing a light interference. The dotted line indicates first internal reflection
- Fig. 3-3** The reflection as a function of wavelength using air gap of 5.0 μm
- Fig. 3-4** Schematic diagram of electro-optical measurement system
- Fig. 3-5** Flow chart of fabrication process
- Fig. 3-6** Schematic of a liquid crystal cell
- Fig. 4-1** AFM images and RMS roughness values of PI, PVA, PS, PSSA, PVP, and PVPD, respectively
- Fig. 4-2** V-T curves of TN cells using rubbed PI, PVA, PS, PSSA, PVP, and PVPD, respectively. The inset shows the normalized V-T curves
- Fig. 4-3** Capacitance dependence on applied voltage for polyimide at strong, medium, and weak rubbing conditions, respectively
- Fig. 4-4** Electro-optical properties of TN cells using rubbed PI at weak, medium, and strong rubbing strengths. The inset shows normalized V-T curves
- Fig. 4-5** Capacitance dependence on applied voltage for PSSA at strong (top) and medium (bottom) rubbing conditions
- Fig. 4-6** Electro-optical properties of TN cells using rubbed PSSA at medium and strong rubbing strengths. The inset shows the normalized V-T curves
- Fig. 4-7** Capacitance dependence on applied voltage for PVP at strong (top) and medium (bottom) rubbing conditions
- Fig. 4-8** Electro-optical properties of TN cells using rubbed PVP at medium and strong rubbing strengths. The inset shows the normalized V-T curves
- Fig. 4-9** Electro-optical properties of TN cells using rubbed PI, PSSA, and PVP at strong rubbing strength. The inset shows the normalized V-T curves
- Fig. 4-10** Capacitance dependence on applied voltage for PVPD at strong (top) and

medium (bottom) rubbing conditions

Fig. 4-11 Experimental geometries of in-plane and out-of-plane asymmetries used for the NEXAFS measurements

Fig. 4-12 Polarization-dependent C K-edge NEXAFS spectra of rubbed PSSA for in-plane asymmetry (top) and out-of-plane asymmetry (bottom). Inset shows the magnification of π orbitals.

Fig. 4-13 Illustration of in-plane phenyl ring orientation (left) and a preferential tilt of phenyl planes by an angle γ from the z axis (right) of PSSA

Fig. 4-14 Polarization-dependent C K-edge NEXAFS spectra of rubbed PS for in-plane asymmetry (top) and out-of-plane asymmetry (bottom)

Fig. 4-15 Polarization-dependent C K-edge NEXAFS spectra of rubbed PVP for in-plane asymmetry (top) and out-of-plane asymmetry (bottom). Inset shows the magnification of π orbitals.

Fig. 4-16 Illustration of phenyl ring orientation (left) and a preferential tilt of phenyl planes by an angle γ from the z axis (right) of PVP

Fig. 4-17 Polarization-dependent C K-edge NEXAFS spectra of rubbed PVPD for in-plane asymmetry. Inset shows the magnification of π orbitals.

Chapter 1

Introduction

1.1 Display Technology

Display technology has expanded incessantly since the last few years of the 21st century, especially for the flat panel displays (FPDs) which are everywhere in our daily lives, for example, mobile phones, camera screens, monitors, televisions, notebooks, traffic signals, and electronic signage [1]. With such great development, display technology becomes indispensable for a human being's life. As a result, human demand impulses the formation and the growth of more and more display technologies. FPD technologies can be divided into several kinds such as Liquid Crystal Displays (LCDs), Plasma Display Panels (PDPs), Light Emitting Diodes (LEDs), Organic Light-Emitting Devices (OLEDs), and Field Emission Displays (FEDs). Each technology has its own strengths and applications. Among such kinds of technology, desired features of thin format, compact size, light weight, high image quality, and reasonable cost can be achieved by LCDs.

1.2 Introduction of Liquid Crystal

Liquid crystalline phase was first discovered by Friedrich Reinitzer [2] in 1888 and the well known term "liquid crystal" (LC) was introduced by Otto Lehmann [3] in 1889. Liquid crystal is an intermediate phase of matter between the crystalline solid and isotropic liquid. There are some different types of liquid crystal phases, also called

“mesophases”, can be distinguished based on their own properties. The illustration of crystal, liquid crystal, and liquid phases is given in Fig. 1-1

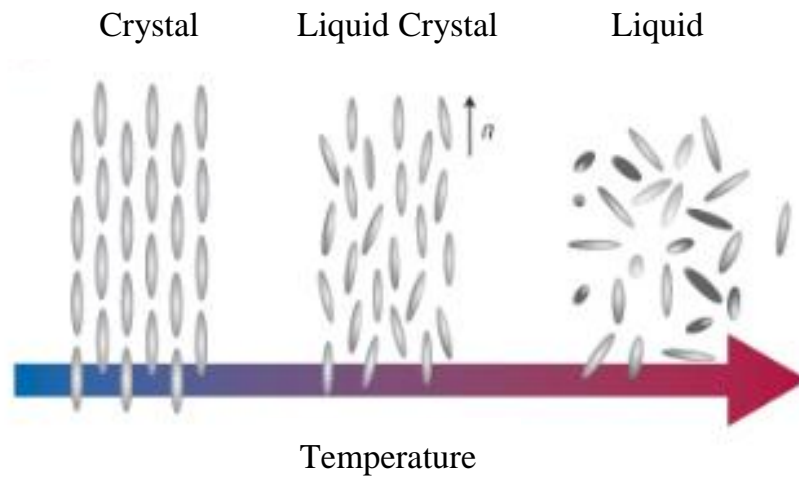


Fig. 1-1 Schematic illustration of crystal, liquid crystal, and liquid phases

Liquid crystals consists of two basic groups: lyotropic phases and thermotropic phases [4]. Lyotropic liquid crystals are formed when a suitable concentration of a material is dissolved in some solvents [5] while thermotropic liquid crystals exhibit temperature dependence of various liquid crystalline phases. Based on the molecular shape of the constituent molecules, thermotropic liquid crystals can be classified into two main kinds: calamitic (rod-like) mesogens and discotic (disk-like) mesogens. Calamitic mesogens are mainly composed of nematic, smectic, and cholesteric.

The change of liquid crystal phase depends on temperature. The molecules are in the isotropic liquid state, having no either orientational order or positional order when the temperature is higher than the clearing point.

Among calamitic mesogens, the nematic phase is the simplest and the most common liquid crystal phase in which the molecules have orientational order but no positional order [6]. The long axis of the molecules reveals preferred direction, orienting along a specific direction, is called liquid crystal director and denoted by the unit vector \vec{n} . The molecules align in parallel directions but not in layers. The

nematic liquid crystals are widely applied into monitors, televisions because of its prominent advantages: small viscosity, fast response time [7-8].

To describe the orientational order of the molecules in nematic liquid crystals, the order parameter is given and defined as below

$$S = \frac{1}{2}(3\cos^2\theta - 1)$$

Where θ is the angle between the molecular axis and the director axis. The order parameter is an average through the whole system, providing a measure of the long-range orientation order. The smaller the fluctuation of the molecular axis from the director axis orientation direction, the closer the magnitude of order parameter is to unity [5]. The order parameter $S = 1$ shows a perfectly orientational order (crystalline phase). Otherwise, the order parameter $S = 0$ expresses no orientational order (isotropic phase). In general, the order parameter of liquid crystal has the typical value in the range of $0.4 < S < 0.7$.

A striking difference between liquid crystal and ordinary anisotropic or isotropic liquid is the existence of a short-range order in the isotropic phase, meaning molecules within a short distance of one another are correlated by intermolecular interactions. Short-range order in the isotropic phase gives rise to critical behavior of the liquid crystals under the effect of externally applied fields [5].

1.3 Liquid Crystal Displays

1.3.1 The fundamental concept of Liquid Crystal Displays

Liquid crystals are widely commercial applied over the last decades in electro-optical flat panel displays, for example, watches, calculators, portable

telephones, notebooks, laptop computers, ect [9]. Nowadays, LCDs have gradually replaced Cathode Ray Tubes (CRTs) in the computer monitor market as well as have dominated displays market in portable instruments because of their great strengths such as small size, low weight, low operation voltage, and low power consumption.

The first generation of liquid crystal displays was dynamic scattering mode displays. However, this type of display is more and more obsolete since the appearance of twisted nematic displays, except for some special applications. The basic difference between these two modes is purely dielectric and non-purely dielectric effect. The dynamic scattering mode is based on the principle of dielectric as well as conductivity alignment while the rest of LC displays including twisted nematic mode is based on purely dielectric effect.

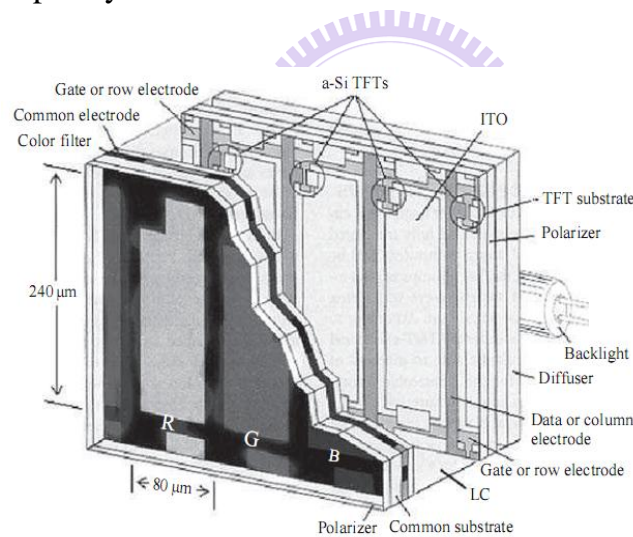


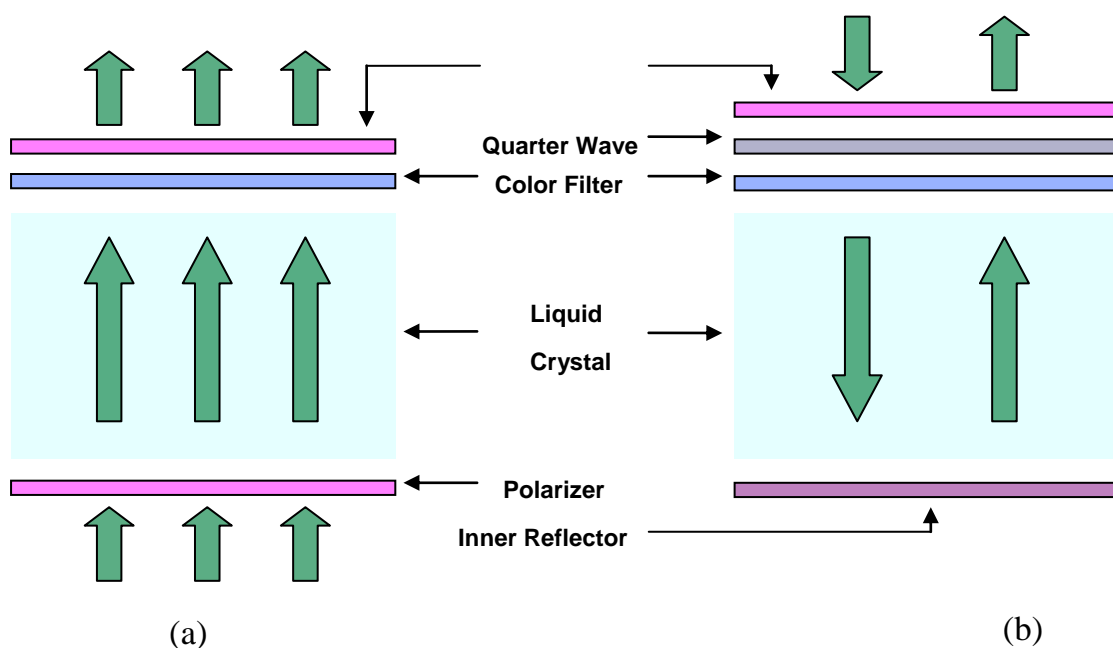
Fig. 1-2 Device structure of transmissive LCD

Liquid Crystal Displays is known as passive electro-optical displays, which can not produce the light by itself but only modulate the light. Liquid Crystal Displays comprises three main types: transmissive, reflective, and transflective. Transmissive LCD was demonstrated by Sharp Corporation in 1989 [10]. A backlight system is very necessary for transmissive LCD to illuminate the LCD panel and the transmission light is controlled by the change of liquid crystal molecular orientation for the purpose

of image display. LCDs are composed of polarizer, color filter, liquid crystal, and backlight as shown in Fig. 1-2.

The displayed images of transmissive LCD are not appropriate for outdoor applications because the ambient light is stronger than emit light from backlight. Hence, the appearance of reflective LCDs [6, 11] is a better choice. Reflective LCDs can be divided into direct-view and projection displays. A direct-view reflective LCD uses ambient light to display the images. Cholesteric liquid crystal materials which can reflect specific wavelength of light were paid much attention in the research of reflective LCDs [6, 12].

A major disadvantage of reflective LCDs is unreadable in dark ambient conditions. Transflective LCD [13] appears like the combination of transmissive LCD and reflective LCD. Transflective LCD uses an inner reflector to reflect ambient light in reflective area while light was displayed by backlight system in transmissive area. Among three kinds of LCDs, transmissive LCD is the most promising candidate for the multimedia display applications due to its simple fabrication process. Fig. 1-3 (a), (b), and (c) show three typical kinds of LCDs.



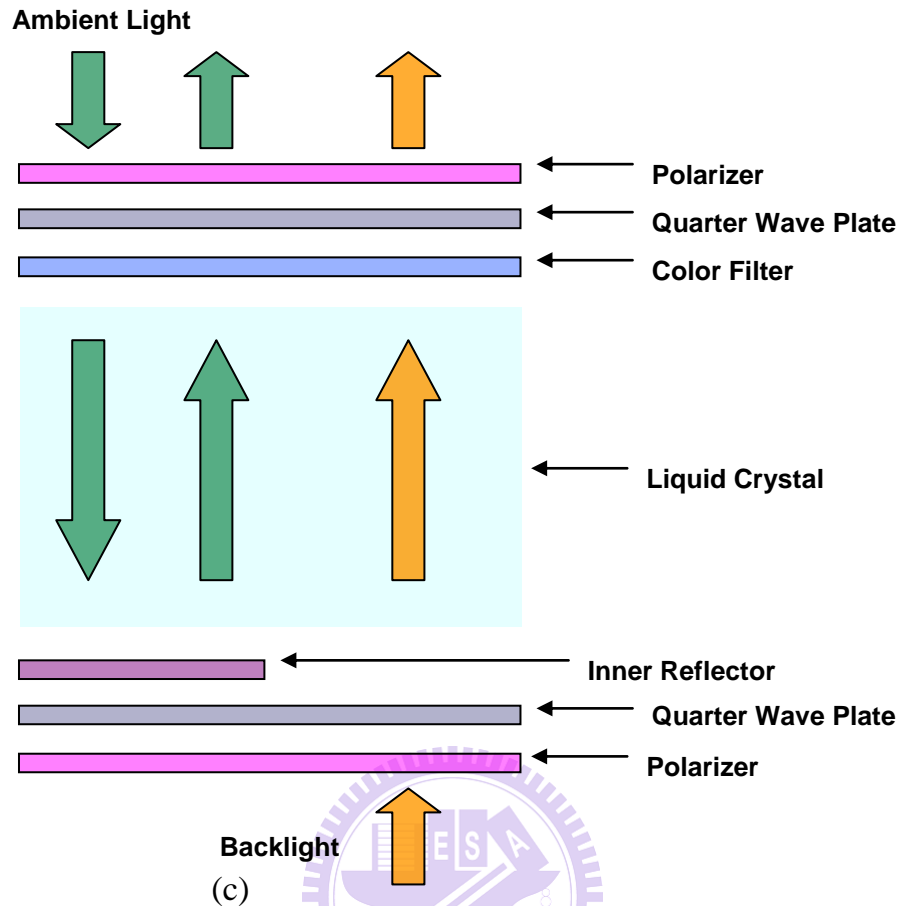


Fig. 1-3 (a) Sketch of Transmissive LCD, (b) Reflective LCD, and
(c) Transflective LCD

The most widespread LCDs applications in transmissive LCDs are the twisted nematic (TN) modes. Like the other modes, twisted nematic mode has particular strengths and weaknesses. High contrast ratio and low driving voltage are main advantages of TN mode. The twisted nematic LCDs have been used extensively to a mass commercial production because of its simple fabrication process, high production throughput, and low production costs. However, slow response time and narrow viewing angle are the critical drawbacks of TN LCDs applications. In this thesis, TN cells will be used to examine the electro-optical characteristics of different alignment materials.

1.3.2 Operation principle of twisted nematic liquid crystal

In twisted nematic [6, 14] liquid crystal displays, the nematic liquid crystal of positive permittivity is used. Figure 1-4 shows the LC director configurations of the normally-white TN cell in the voltage-off (on state) and voltage-on (off state) states.

The TN cell is placed between two crossed polarizers. In the voltage-off state, the top LC directors are parallel to the transmission axis of the top polarizer while the bottom LC alignment direction is twisted 90 degree and parallel to the transmission axis of the bottom analyzer. The incident linearly polarized light follows the molecular twist and transmits through the crossed analyzer, corresponding to a bright state. When the voltage is applied through the whole cell, the liquid crystal directors are reoriented along the electric field direction (perpendicular to the substrates), from homogeneous alignment to homeotropic alignment, except for the boundary layers. The incoming light experiences phase change and is blocked by the crossed analyzer, resulting in a dark state.

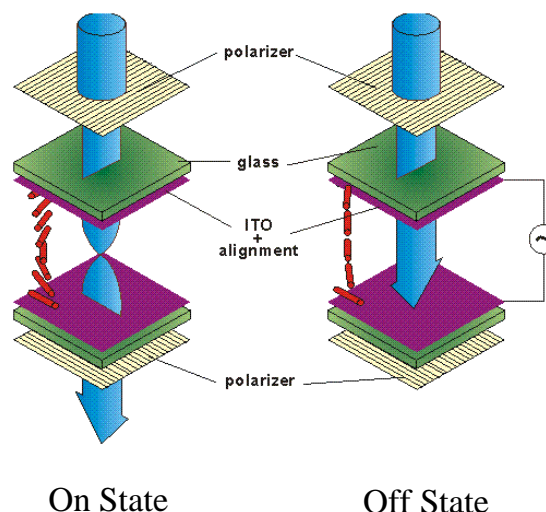


Fig. 1-4 The operation principle of normally white twisted nematic

1.4 Liquid Crystal Alignment

In liquid crystal displays devices, alignment layer is to align liquid crystal molecules toward the preferential direction on its surface. A uniform and defect free alignment of the liquid crystal molecules on the surface of alignment layers is prerequisite condition for the quality of liquid crystal displays since LC devices are operated through the variation of nematic liquid crystal molecular orientations. Fig. 1-5 illustrates typical orientations of LCs induced on alignment layer.

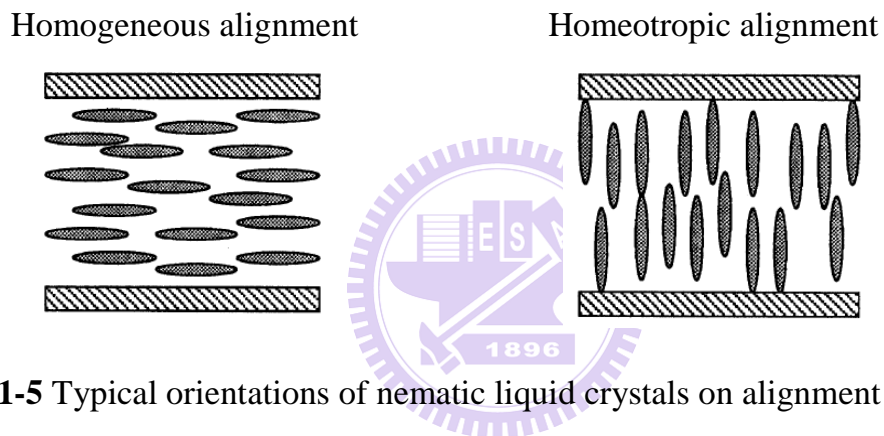


Fig. 1-5 Typical orientations of nematic liquid crystals on alignment layer

The aligning ability of alignment materials depends on several following elements, namely, alignment layers' direction order, interaction energies between LC and surface of alignment layer, and effective LC order.

2.4.1 Alignment techniques

Homogenous alignment of liquid crystal molecules on the surface of alignment layers can be achieved by a variety of methods. It could be highly uniform with desirable alignment parameters, such as selective pretilt angle and strong anchoring energy which play very important roles to the electro-optical performance of LCD

devices. In general, liquid crystal alignment techniques can be divided into two main types, contact and non-contact method. Mechanical rubbing represents contact alignment method. Non-contact alignment method consists of oblique evaporation technology [15], photoinduced surface alignment [15-16], plasma treatment [17-21], and ion beam treatment [22-23]. Mechanical rubbing is adopted as the liquid crystal alignment method in this thesis.

2.4.2 Alignment materials

The quality of LCDs depends not only on the alignment technique but also on the alignment materials. A diversity of materials is tested as alignment materials for rubbing treatment such as polyvinyl alcohol, nylon, acrylics polymers, vinyl polymers, polyimide, ect. Among these materials, polyimide (PI) has been the dominate alignment material in the LCD market due to its outstanding benefits, for example, stability, superior electric characteristics, strong aligning ability, good electro-optical property, strong anchoring energy. However, the baking temperature over 200⁰ C is the critical drawback which limits the applications of polyimide for flexible substrates in flat panel liquid crystal displays.

In this research, different polymers having low baking temperature are tested as alignment materials.

1.5 Motivation and Objective

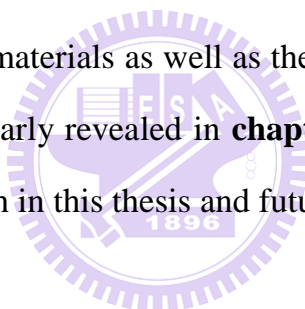
The rubbing method on polyimide surface has dominated the alignment films' preparation for LCDs production. However, its major limitation is curing temperature over 200⁰C that is required for the film preparation. This is a considerable

disadvantage in applying polyimide into various flexible substrates.

As a result, new alignment materials for low temperature process are the emerging needs of energy conservation. In this thesis, various polymers containing distinct functional groups induced by mechanical rubbing technique such as polystyrene sulfonic acid (PSSA), poly (4-vinylphenol) (PVP), and polyvinylpyrrolidone (PVPD) are tested as new liquid crystal alignment materials in comparison with known materials, including polyimide (PI), polyvinyl alcohol (PVA), and polystyrene (PS). The process temperature for these materials can be as low as 110⁰C. The fabrication process of LC cells will be described in detail in the chapter 4. The commercial available indium-tin oxide (ITO) glasses are cleaned by standard process. After that, polymers tested as liquid crystal alignment layers are coated on the clean ITO glasses. The surface morphology of these new materials is observed by AFM. These alignment layers are treated by the mechanical rubbing method. Two substrates with their rubbing directions perpendicular each other are assembled to make TN cells. The cell gap of TN cell is controlled approximately 5 μm by spacer and the space between two substrates is filled with the nematic LC E7 (Merck). The electro-optical performances of TN cells made from different alignment materials are investigated. Furthermore, antiparallel cells filled with the mixture of LC and dye are prepared to measure the order parameter. The polar anchoring energy is also examined to evaluate the aligning ability of new alignment materials. Moreover, the orientational order of chemical functional groups of alignment layers will be studied by surface-sensitive and polarization-dependent near X-ray absorption fine structure spectroscopy.

1.5 Organization of This Thesis

This thesis includes five main chapters. **Chapter 1** introduces general information about liquid crystal displays. In **chapter 2**, the fundamental principle of PEEM using Synchrotron Radiation Source and the alignment mechanism of mechanical rubbing method are presented in detail. **Chapter 3** describes measurement instruments which are used to examine the surface morphology, the order parameter, the electro-optic characteristics of TN cells, the polar anchoring energy, the preferential orientation order at the surface of alignment materials induced by rubbing treatment such as AFM, UV-Visible Spectroscopy, Electro-optical measurement system, LCAS, NEXAFS, respectively. The experimental results and discussion about the performance of TN cells using different alignment materials as well as the molecular orientation at rubbed alignment layer surfaces are clearly revealed in **chapter 4**. Finally, **chapter 5** gives a conclusion of the whole research in this thesis and future work.



Chapter 2

Principle of Liquid Crystal Alignment and Near Edge X-ray Absorption Fine Structure (NEXAFS) Spectroscopy

2.1 Mechanical Rubbing Technique

It can not be denied that a variety of surface treatments are able to obtain a homogenous alignment of LC layer. Among the possible surface treatments, mechanical rubbing of polymer surfaces is the most popular technique used to align liquid crystal molecules for the mass production in the LCD market. Rubbing method has been dominated for alignment technologies in terms of its simplicity, convenience and low-cost products. In the mechanical rubbing process, the surface of alignment layers is rubbed with a cloth during the rubbing procedure. The direct contact between the surface of alignment layer and the cloth is the main reason causing static electricity and dust which are serious problems of rubbing process, restricting the expansion of large size LCDs products.

2.1.1 Rubbing strength

Mechanical rubbing is found out as an effective method to align liquid crystal molecules over many decades by Mauguin [24]. Mechanical rubbing is generally carried out by moving the substrate with a constant velocity under a rotating roller covered with a velvet cloth, as depicted in Fig. 2-1.

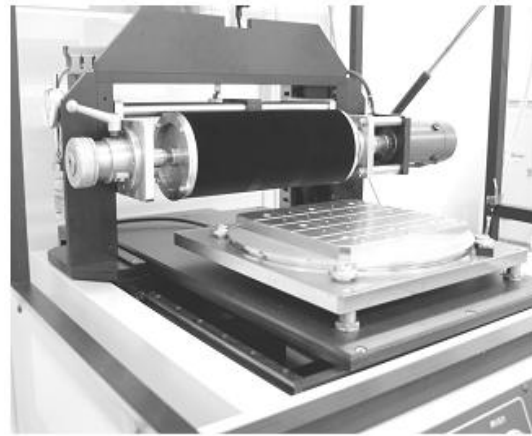


Fig. 2-1 Photograph of rubbing machine

The rubbing force is varied with the rubbing process parameters such as the roller diameter, the rotation speed, the substrate advancing speed, number of rubbings, and the pile impression (the depth of the rubbing cloth pressed down by roller), as shown in Fig. 2-2. The rubbing strength (RS) is defined as below [25]:

$$RS = NM(2\pi rn / V - 1)$$

Where N is the number of rubbings, M is the pile impression (mm), n is the rotation speed of the roller (s^{-1}), V is the advancing speed of the substrate (mm/s), and r is the radius of the roller (22.5 mm). The RS is given in mm unit.

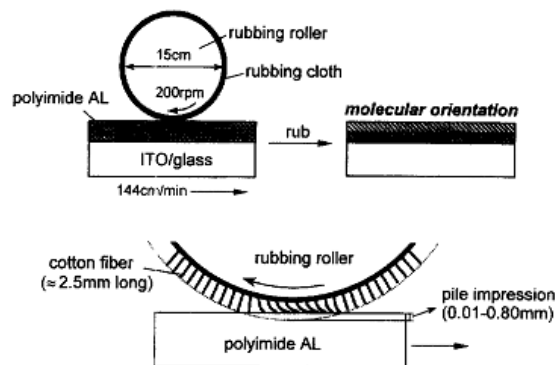


Fig. 2-2 Schematic of mechanical rubbing

Rubbing parameters strongly influence the performance of LC devices, particularly, the electro-optical properties, pretilt angle, and anchoring energy [25].

File impression has great effects on rubbed alignment layers. The number of rubbings is related to the rubbing density and weak rubbing density causes poor electro-optical characteristics and non-uniform alignment.

2.1.2 Alignment mechanism induced by rubbing method

The understanding of alignment mechanism induced by rubbing treatment is not only an interesting theory but also an important industrial issue. A series of questions are proposed to satisfy the curiosity about alignment mechanisms as a result of rubbing treatment. What happens to the alignment layer as its surface is rubbed? Why such rubbed polymer surfaces can align liquid crystal molecules in a specific direction? Why can only some polymers produce good alignment? Many hypotheses are pointed out to explain such mysterious phenomenon. In the early period, one possibility was given that aligning ability of LC molecules on the surface of alignment layer was due to the grooves or scratches induced by the rubbing process. The LC molecules will reorient along the grooves created on rubbed alignment layer. Thus, the surface morphology of the rubbed surfaces was particularly considered, which was examined by scanning tunnel microscope (STM) and atomic force microscope (AFM) [26-29].

In the early stages, the alignment mechanism induced by rubbing treatment was explained based on the appearance of grooves or scratches on the rubbed surfaces [30]. However, such a mechanism is impossible to explain the behavior of alignment in many cases. Strong aligning ability of some rubbed polymer surfaces was found out even having no evidences of scratches or grooves [31].

Another concept for the alignment mechanism was that polymer chain orientation can act to align liquid crystal [31]. The polymer film was caught between one stationary (substrate) plane and the other moving (the fiber contact area) plane. As a

result, the polymer exhibited a shearing force. Shear deformation created by such shearing force can be obtained by rubbing process, as illustrated in Fig. 2-3. Fig. 2-3 (a) describes a polymer film contacting with a moving fiber of rubbing material. Fig. 2-3 (b) depicts a form of deformation under a shearing force. Fig. 2-3 (c) and (d) illustrate an extreme parallelogram form produced by the effect of large shear deformation. It was known that the orientation of the polymer chains could induce birefringence which is due to the difference in refractive index for light polarized parallel and perpendicular to the polymer chains. Fig. 2-4 shows the plot of retardation of different materials induced by rubbing method. All rubbed surfaces exhibited positive retardation, except for rubbed PS showing negative retardation. Positive retardation pointed out that the slow axis was parallel to direction of rubbing and negative retardation indicated that the slow axis perpendicular to rub axis.

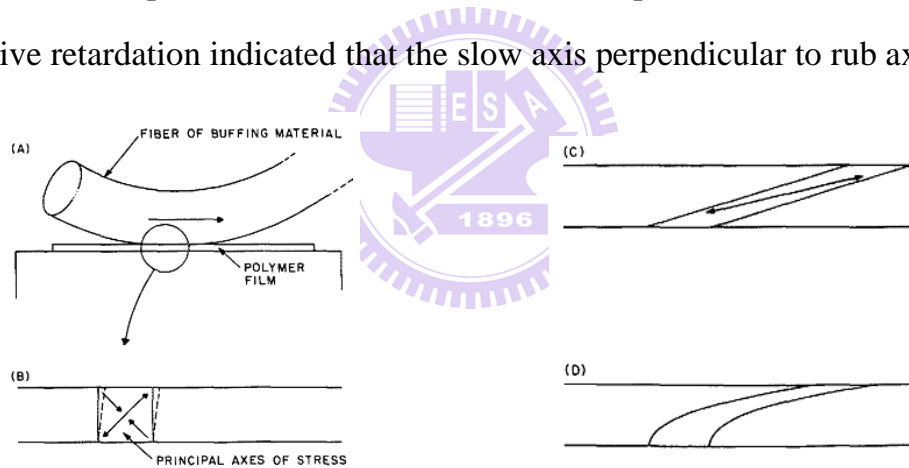


Fig. 2-3 The geometry of shear deformation in cross section

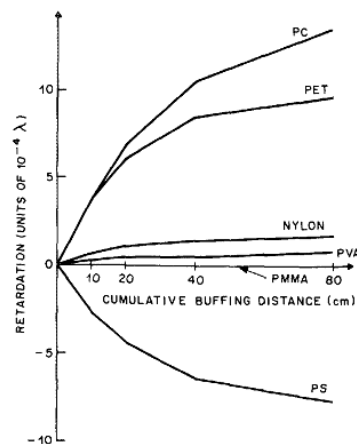


Fig. 2-4 Plot of retardation induced by rubbing

The existence of birefringence demonstrates the orientation of the polymer chains induced by the rubbing method. Such orientation happened through a shearing deformation of the polymer film and this deformation accumulated in narrow streaks during the rubbing process. In this hypothesis, the streak accumulation and shearing force were the main mechanisms of the rubbing treatment.

Table 2.1 Alignment obtained with various rubbed polymer films

Polymer	Smectics		Nematics	
	Aligns	No alignment	Aligns without defects, sheet nucleation	Aligns with defects, point nucleation
Polyethylene-terephthalate	×		×	
Nylon 6/6	×		×	
Polyvinyl alcohol	×		×	
Polyformaldehyde		×		×
Polystyrene		×		×
Polycarbonate		×		×
Polymethylmethacrylate		×		×
Bare glass		×		×

Table 2.1 describes the aligning ability of various rubbed polymer films. Those rubbed polymer surfaces were divided into two categories. The first category included rubbed films having strong aligning ability while the second category consisted of rubbed polymers causing weak alignment in the nematic material. The polymers of the first category were highly crystalline materials, while those of the second category were strongly amorphous. The crystallinity of the polymer was considered as the difference in aligning ability of these two categories. Therefore, both polymer chain orientation and polymer crystallinity are the necessary conditions for alignment induced by rubbing treatment in this hypothesis.

In company with the appearance of surface-sensitive techniques, thorough insights into the alignment mechanism have been gradually understood obviously. In general, liquid crystal alignment originates from symmetry breaking at the surface of the polymer substrate [32]. A microscopic bond orientation model for liquid crystal

alignment by rubbed polymer surfaces, examined by surface-sensitive and polarization dependent near X-ray absorption fine structure (NEXAFS) measurements, was proposed by J. Stohr group [32-34]. Based on NEXAFS spectra, Stohr groups proposed the LC alignment model based on the existence of a statistically significant unidirectional bond asymmetry at polymer surface. In this model, the LC direction followed the preferential orientation of the phenyl rings which was explained in terms of the preferential chain segment alignment through a pulling action of the rubbing cloth fibers. This model demonstrated that the LC alignment was not related to the crystalline order of rubbed polymer surfaces.

NEXAFS spectroscopy has been a powerful tool to study the origin of alignment process.

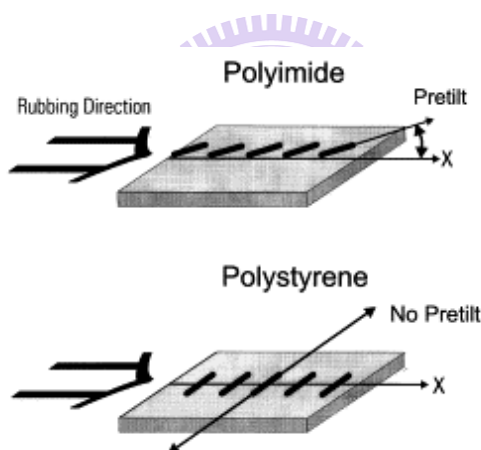


Fig. 2-5 Liquid crystal orientation on rubbed surfaces

To have deeper viewpoints into the alignment process, two different kinds of materials are chosen to examine by NEXAFS measurements, rubbed polyimide and rubbed polystyrene, for a special reason. Rubbed surfaces of these two materials show the opposite behavior of their aligning abilities. Rubbed polyimides align liquid crystal molecules along the rubbing direction with the pretilt angle points toward the rubbing direction. In contrast, rubbed polystyrene aligns LCs perpendicular to the rubbing direction with zero pretilt angle [35-36], as indicated in Fig. 2-5. NEXAFS

measurements clearly indicate the preferential in-plane and out-of-plane asymmetries at the rubbed polymer surfaces.

The π orbitals of phenyl rings have a preferred in-plane alignment along the direction perpendicular to the rubbing direction. In the case of rubbed polystyrene, by contrast, there is an increase in the number of phenyl rings with their π orbitals along the rubbing direction, as illustrated in Fig. 2-6. The liquid crystal molecules are understood to be preferentially oriented with their long axis perpendicular to the π orbitals of the phenyl rings or C=O groups [32-34]. Thus, LC molecules align along the rubbing direction for rubbed polyimide and perpendicular to the rubbing direction for rubbed polystyrene.

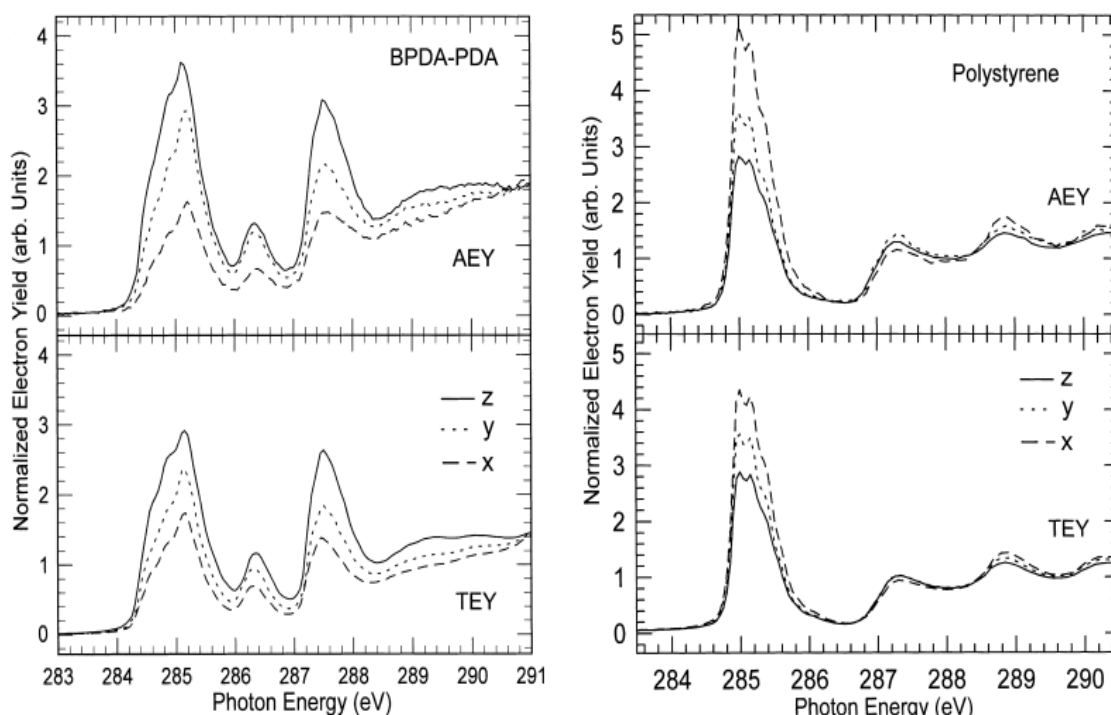


Fig. 2-6 NEXAFS spectra recorded by Auger (AEY) and total (TEY) electron yield for rubbed BPDA-PDA polyimide (in the left) and rubbed 96K polystyrene (in the right), with the electric field parallel to x, y and 20° from the z axis

2.2 Near-Edge X-ray Absorption Fine Structure (NEXAFS) Spectroscopy

2.2.1 Elliptically Polarized Undulator (EPU)

The Sasaki type Elliptically Polarized Undulator (EPU) with 5.6 cm magnets is used for the BL05B2 beamline. The elliptically polarized undulator is capable of both delivering high photon flux with energy in the range of 60eV – 1400eV and producing elliptically, right or left circularly, or linearly polarized light.

The elliptically polarized undulator is composed of two pairs of permanent magnets arrayed above and below the electron beam [37-38]. The energy and polarization state of light can be varied by changing the gap width between the upper pair of magnets and the lower pair of magnets (gap shift) as well as shifting the relative position between right and left magnets in each pair (phase shift). Fig. 2-7 illustrates the way EPU produces the linearly polarized light which is used in my experiment.

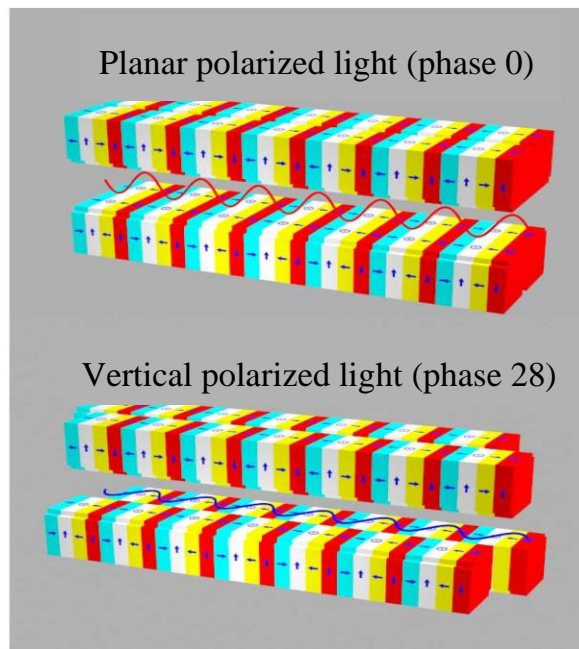


Fig. 2-7 The formation of linearly polarized light by EPU

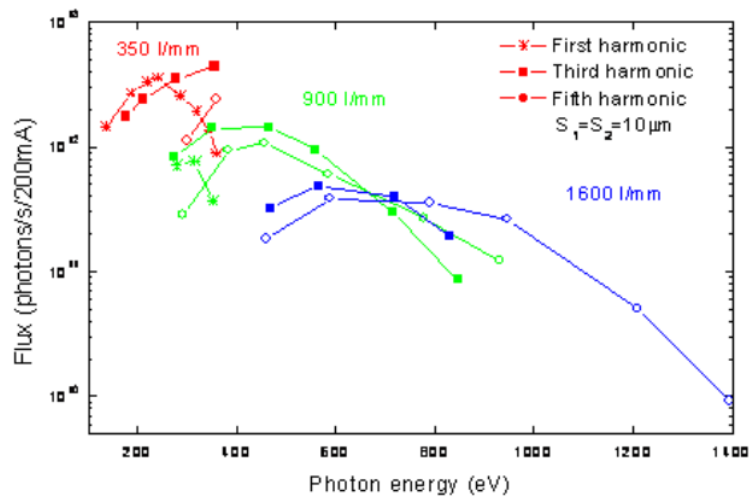
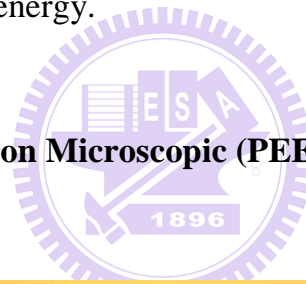


Fig. 2-8 Experimental photon flux spectrum of the EPU beamline

Fig. 2-8 describes photon flux spectrum of EPU as well as the used corresponding grating as a function of photon energy.



2.2.2 Photoemission Electron Microscopic (PEEM)



Fig. 2-9 PEEM station at EPU

Fig. 2-9 is a typical photograph of Photoemission Electron Microscopic (PEEM) end station at EPU beamline in NSRRC. The PEEM [39] end station is located at beamline BL05B2. PEEM is a “photon in – electron out” technique. X-ray PEEM (X-PEEM) using linearly polarized soft X-ray is determined to investigate the molecular orientation of rubbed polymer surfaces by combining high spatial resolution imaging with near edge X-ray absorption fine structure (NEXAFS) spectroscopy [40-41]. NEXAFS measurements used in my experiment will be presented in detail later.

2.2.3 The operation principle of NEXAFS measurements

The microscopic origin of liquid crystal alignment on rubbed polymer surfaces has been discussed since its discovery in 1911 [42]. The alignment mechanism is of significant technological problem because flat panel displays are mainly based on the light transmission from the back to the front of display through the orientation changes of liquid crystal molecules [43-45]. As a result, discovering the origin of the alignment mechanism has become imperative issue, challenging and attracting too much attention to researches.

A series of diverse measurement techniques has been suggested to investigate the molecular orientation at rubbed polymer surfaces, for example, atomic force microscope observation [27], bulk-sensitive optical measurements [31, 46], infrared (IR) birefringence studies [31, 47], surface sensitive studies using optical second-harmonic generation (SHG) [48], X-ray photoelectron spectroscopy (XPS), X-ray diffraction [49], the near edge X-ray absorption fine structure [32-34, 40, 50-63], and grazing incidence X-ray scattering (GIXS) [64-66] techniques. Among these technologies, polarization-dependent near edge X-Ray absorption fine structure

spectroscopy has been applied to the study of liquid crystal alignment in recent years.

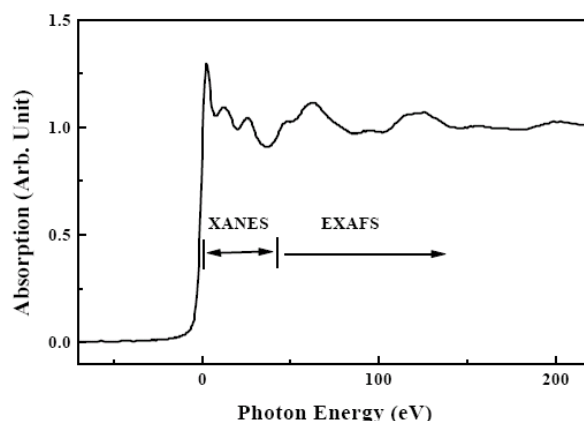


Fig. 2-10 Illustration of absorption region of XANEX and EXAFS

NEXAFS is also called X-ray absorption near edge structure (XANES). The term NEXAFS is typically used for soft X-ray absorption spectra and XANES for hard X-ray spectra. Near edge X-Ray absorption fine structure spectroscopy mentions to the absorption fine structure close to an absorption edge, about the first 30eV above the actual edge while extended X-ray absorption fine structure (EXAFS) refers the higher absorption energy region, as illustrated in Fig. 2-10. NEXAFS region usually shows the largest variations in the X-ray absorption coefficient and is often dominated by intense, narrow resonances.

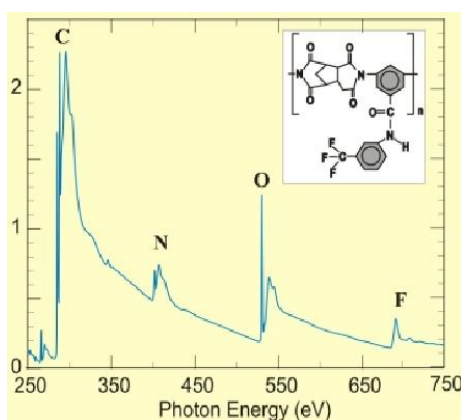


Fig. 2-11 NEXAFS spectrum of different elements in a polyimide polymer

NEXAFS is element-specific with respect to different energies of the X-ray absorption edges of different elements, as shown in Fig. 2-11. NEXAFS is of high sensitivity to the chemical bonding environment of absorbed atoms. Furthermore, these fine structures vary with different positions and the surroundings of absorbed atoms, as seen in Fig. 2-12. Overall, NEXAFS has the ability of partial chemical bonding environmental identification.

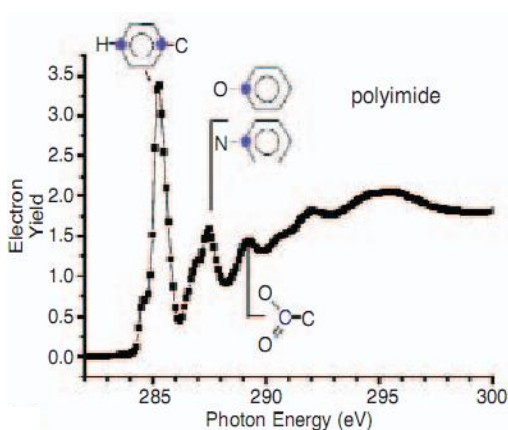


Fig. 2-12 Near edge X-ray absorption fine structure spectrum (Carbon K-edge)

Polarization dependence is another remarkable benefit of NEXAFS spectroscopy due to the anisotropy of transition dipole moments. In NEXAFS measurements, linearly polarized X-rays are the best light source for the covalent systems like low-Z molecules, macromolecules and polymers, which possess directional bonds [41]. In this case, the electric field vector of the X-ray is like as a "search light" that can seek the direction of chemical bonds of the atom selected by its absorption edge [67].

Fig. 2-13 shows polarization dependent NEXAFS spectra for benzene chemisorbed on Ag (110), demonstrating the ability of the molecular orientations. Benzene (C_6H_6) has unoccupied orbitals of σ and π symmetries which are oriented in and perpendicular to the ring plane, respectively. When the electric field vector E aligns along the surface normal, absorption intensity due to the out-of-plane π orbitals

are enhanced and when the electric field vector E is parallel to the surface, resonant intensity due to the in-plane σ orbitals are dominant. This evidence confirms that benzene lies down on the Ag surface. The intensity of absorption is proportional to the amount of the specific chemical bonding. By changing the incident angle and the direction of polarization, the information of directional chemical bonding can be obtained.

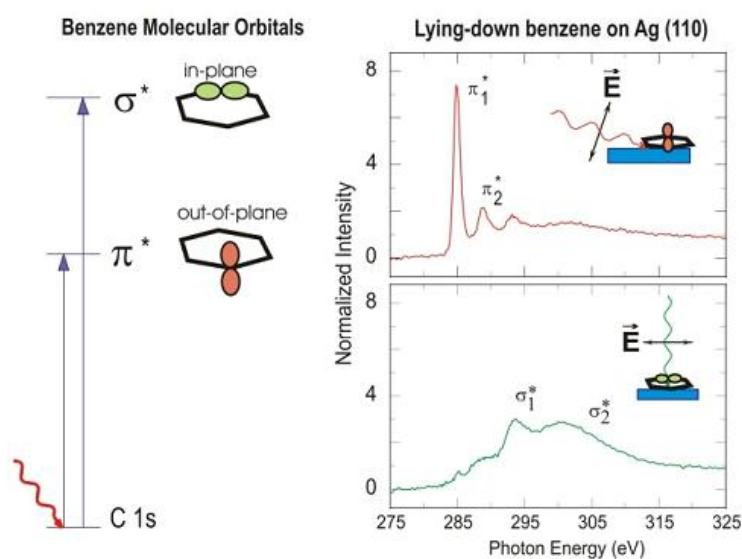


Fig. 2-13 Polarization dependent NEXAFS spectra of benzene chemisorbed on Ag (110)

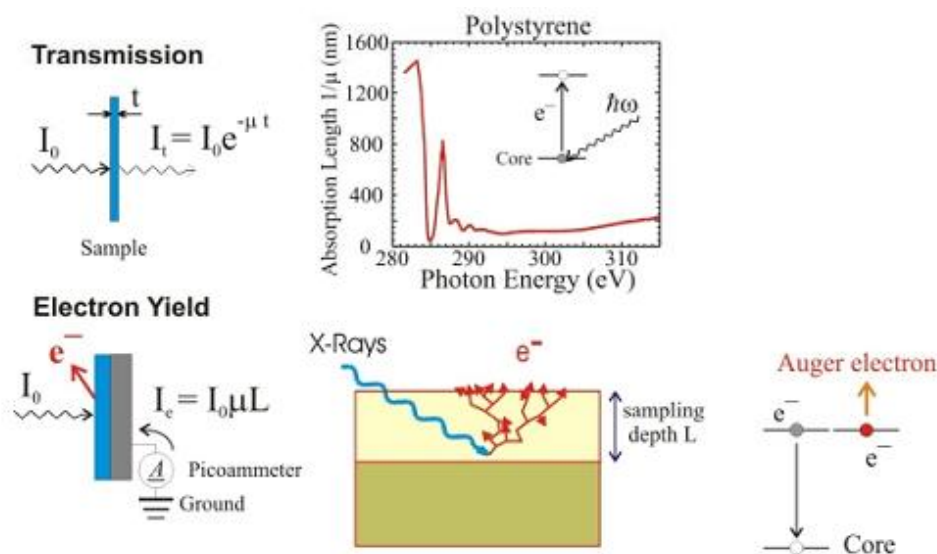


Fig. 2-14 Two techniques to record X-ray absorption spectra

NEXAFS spectroscopy is one of the operation modes of photoelectron emission microscopy. Two main ways used to record NEXAFS spectra are transmission (also called total electron yield) and electron yield (often called Auger electron yield) measurements, as depicted in Fig. 2-14 [67]. The sampling depth in total electron yield (TEY) spectra is estimated to be about 10 nm, while Auger electron yield (AEY) spectra probe only the first nanometer from the surface [58, 67]. Total electron yield technique is studied in this thesis.

The operation principle of NEXAFS is involved the excitation of core electrons, as described in Fig. 2-15. NEXAFS spectra are formed by resonances arising from transitions from the 1s core level to unoccupied molecular orbitals of π^* and σ^* symmetries, corresponding to peaks observed in NEXAFS spectra. Since such states are specific to the bonding within different functional groups, NEXAFS spectra are possible to probe the electronic and magnetic properties of the empty valence levels as well as the chemical composition of polymers [40].

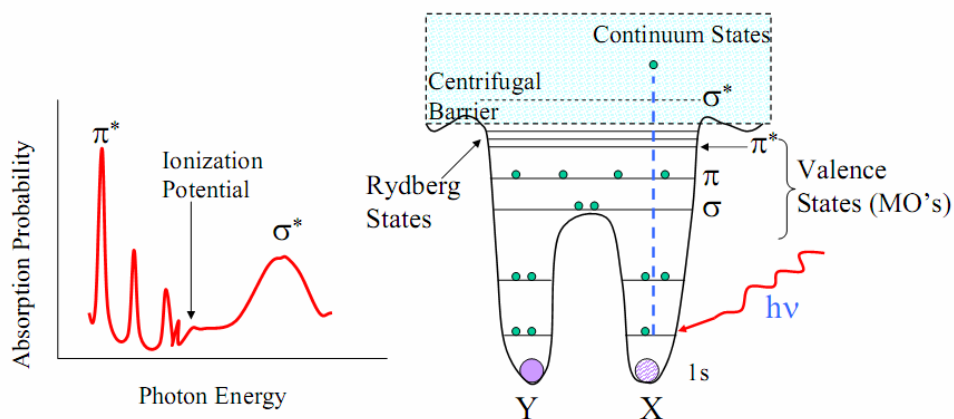


Fig. 2-15 Schematic diagram of a diatomic molecule

Chapter 3

Measurement Instruments and Sample Fabrication

3.1 Introduction

In this chapter, measurement instruments which are used to investigate the performance of alignment materials are described in detail. The surface uniformity of each alignment material is tested by Atomic Force Microscope (AFM). The aligning ability of alignment materials are presented through the order parameter which is measured by UV-Visible Spectroscopy. Besides, Electro-Optical Measurement System is used to examine the electro-optic characteristics of TN cells. The polar anchoring energy which affects directly the electro-optic properties is measured by Liquid Crystal Analysis System (LCAS). Moreover, NEXAFS spectroscopy supplies us the information about the preferential orientation order at the surface of alignment materials induced by rubbing treatment.

3.2 Atomic Force Microscope (AFM)

Atomic Force Microscope (AFM) [68] is composed of a sharp tip mounted at the end of a flexible micro-scale cantilever spring to probe the sample surface. The cantilever is often silicon or silicon nitride with radius on the order of nanometers. When the tip approaches the specimen surface, there is appearance of an interaction force between the tip and the specimen, can be explained by Hooke's law. This force

creates deflection or shift in resonant frequency. The deflection is measured by using a laser spot reflected from the top of the cantilever into an array of photodiodes. To display an image, the interaction between the sample and the tip is mapped to the monitor as a function of position mechanically scanning the sample relative to the tip in a raster pattern into the photo-detector. By detecting the difference in the photo-detector output voltages, changes in the cantilever deflection or oscillation amplitude are determined. A schematic diagram of this mechanism is depicted in Fig 3-1.

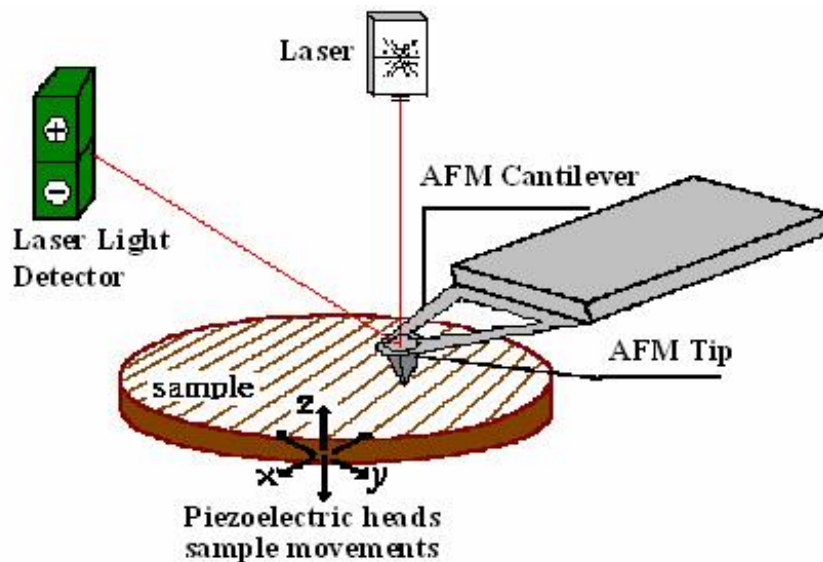


Fig. 3-1 Concept of AFM and the optical lever

There are two major operation modes of AFM:

a. Contact mode

Contact mode is the most common method to operate the AFM in which the tip and the sample remain in close contact as the scanning proceeds. One of the disadvantages of remaining in contact with the sample is that there exists a large lateral force on the sample as the tip is dragged on the substrate.

b. Tapping mode

Tapping mode consists of oscillating the cantilever at its resonance frequency (typically hundreds of kilohertz) and positioned above the surface so that it only taps the surface for a very small fraction of its oscillation period. The laser deflection method is used to detect the root-mean-square (RMS) amplitude of cantilever oscillation. The benefit of tapping mode over contact mode is that it eliminates the lateral, shear forces presented in contact mode, which enables tapping mode to image soft, fragile, and adhesive surfaces without damaging them. In this thesis, the tapping mode is used.

3.3 UV-Visible Spectrometer

3.3.1 Cell Gap Measurement System

For liquid crystal displays, the thickness of cell gap influences seriously the optical performance of the LC cell. Therefore, the cell gap measurement has to be understood in advance as the following procedure of the measurement. The measurement instrument used to measure the cell gap is UV/Vis spectrometer Lambda 950 from Perkin Elmer, and the principle of this method is presented as follow.

UV/Vis spectrophotometer Lambda 950 is operated in the range from visible to ultraviolet spectral with the resolution smaller than 0.17 nm. UV/Vis spectrophotometer is useful for a diversity of applications such as determining the absorption, transmittance, and reflection of materials.

The basic concept of the measurement method is based on the interference of light reflected by the two reflecting surfaces [69-70], as illustrated in Fig. 3-2. The coefficient of reflection R_1 is defined as the ratio of the light reflected by surface 1 to the incident light. Besides, R_2 is the reflection coefficient of surface 2.

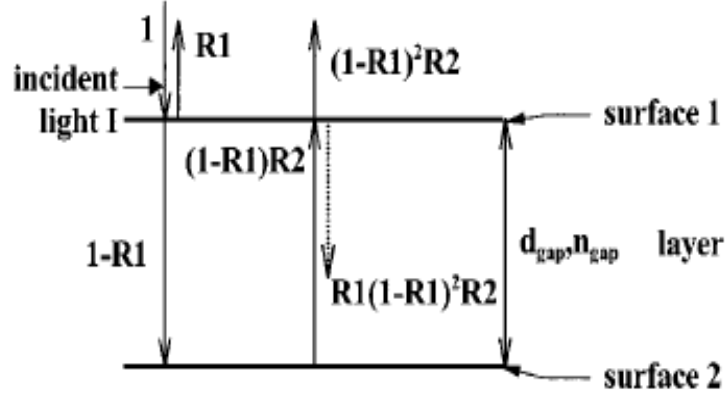


Fig. 3-2 Two reflecting surfaces separated by a layer causing a light interference. The dotted line indicates first internal reflection

We assume the total incident light is $I = \cos\omega t$ and there is no absorption of light at surface 1 and 2. The total reflected light R can be written as

$$R = R_1 \cos\omega t + \sum_{k=1}^{\infty} R_1^{k-1} R_2^k (1-R_1)^{1+k} \cos\omega(t - kt_0) \quad (3-1)$$

Where $\omega = 2\pi c n_{gap} / \lambda$ and $t_0 = 2d_{gap} n_{gap} / c$, c is the speed of light in the vacuum, λ is the wavelength, d_{gap} is the thickness of the layer, n_{gap} is the refractive index of the layer.

The cosine factors in Eq. 3-1 for $k > 1$ are due to internal reflections. Since $R_1 < 1$ and $R_2 < 1$, the magnitude of the cosine factors for $k > 1$ is much smaller than that for $k=1$. As a result, the internal reflections can be neglected, leading to

$$R = R_1 \cos\omega t + (1-R_1)^2 R_2 \cos\left(\omega t - \frac{4\pi n_{gap} d_{gap}}{\lambda}\right) \quad (3-2)$$

Thus the reflected spectrum is

$$|R(\lambda)|^2 = R_1^2 + [(1-R_1)^2 R_2]^2 + 2R_1(1-R_1)^2 R_2 \times \cos(4\pi n_{gap} d_{gap} / \lambda) \quad (3-3)$$

The periodic term in Eq. 3-3 causes an interference pattern. The periodicity of the reflected interference spectrum determines the optical thickness of the cell gap,

$n_{gap}d_{gap}$.

If λ_1 and λ_2 are the two wavelengths showing extrema in Eq. 3-3, then $\cos(4\pi n_{gap}d_{gap}/\lambda) = \pm 1$ for $\lambda = \lambda_1$ and $\lambda = \lambda_2$. Hence

$$2n_{gap}d_{gap} = k_1\lambda_1/2 \quad (3-4)$$

$$2n_{gap}d_{gap} = k_2\lambda_2/2 \quad (3-5)$$

Where k_1 and k_2 are natural numbers. We suppose $\lambda_1 > \lambda_2$, then

$$k_2 = k_1 + x \quad (3-6)$$

In which x is a natural number.

Based on Eq. 3-4, Eq. 3-5, and Eq. 3-6, we can obtain

$$n_{gap}d_{gap} = \frac{x\lambda_1\lambda_2}{4(\lambda_1 - \lambda_2)} \quad (3-7)$$

The value of x-1 defines the number of extrema in $|R(\lambda)|^2$ between two wavelengths λ_1 and λ_2 . It is better to choose the distance x between the two extrema as large as possible in order to improve the accuracy of the calculation of $n_{gap}d_{gap}$. An example of the measurement of a cell with the cell gap $5 \mu m$ is shown in Fig. 3-3.

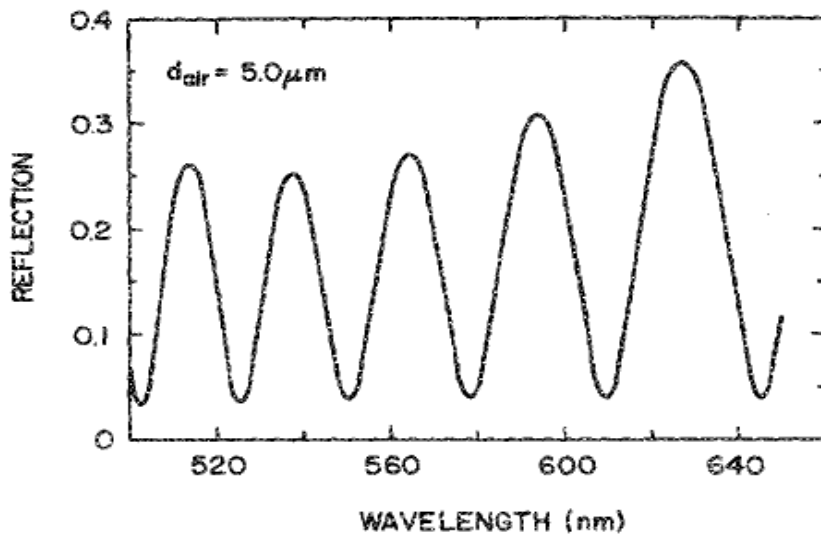


Fig. 3-3 The reflection as a function of wavelength using air gap of $5.0 \mu m$

3.3.2 Order parameter Measurement

Besides measuring the cell gap of LC cell, UV/Vis spectrometer Lambda 950 is also used to determine the order parameter for various liquid crystal alignment materials. The principle of order parameter measurement is described as below

$$S = \frac{A_{//} - A_{\perp}}{A_{//} + 2A_{\perp}} \quad (3-8)$$

$$A_{//} = -\log \frac{I_{//}}{I_o} \quad (3-9)$$

$$A_{\perp} = -\log \frac{I_{\perp}}{I_o} \quad (3-10)$$

Where S is the order parameter.

$A_{//}$, A_{\perp} , $I_{//}$, I_{\perp} are the optical densities (absorbances) and transmittances when the liquid crystal alignment direction of antiparallel cell is parallel and perpendicular to the transmission axis of polarizer, respectively.

I_o is the transmittance before the incoming polarized light goes through the antiparallel cell.

3.4 Electro-Optical Measurement System

The electro-optical measurement system is described in Fig. 3-4. This optical system is responsible for the measurement of V-T characteristics. He-Ne laser is the light source in this system. The intensity of the laser source can be reduced within the acceptable range of the photodetector by using a 10% ND filter. The LC cell is put between a polarizer and an analyzer. The LC cell is driven by a waveform generator WFG500 from FLC Electronics AB which is connected with computer through GPIB interface. Any waveforms can be designed with the maximum output voltage for

$\pm 100\text{V}$ and the minimum pulse width for 200ns. The moderate unpolarized light becomes a polarized light after passing through the polarizer and then enters the LC cell. The LC cell acts as a phase modulator, changing the phase of the incident polarized light by retardation $\Delta n \cdot d$ (Δn is the birefringence of LC and d is the thickness of LC). After that, the modulated light goes through the analyzer and the optical signals output are obtained by the photodetector PIN 20 from FLC Electronics AB as well as observed with the oscilloscope from Tektronix or the multimeter from Keithley. The V-T curve is recorded by using bipolar square wave 1 kHz.

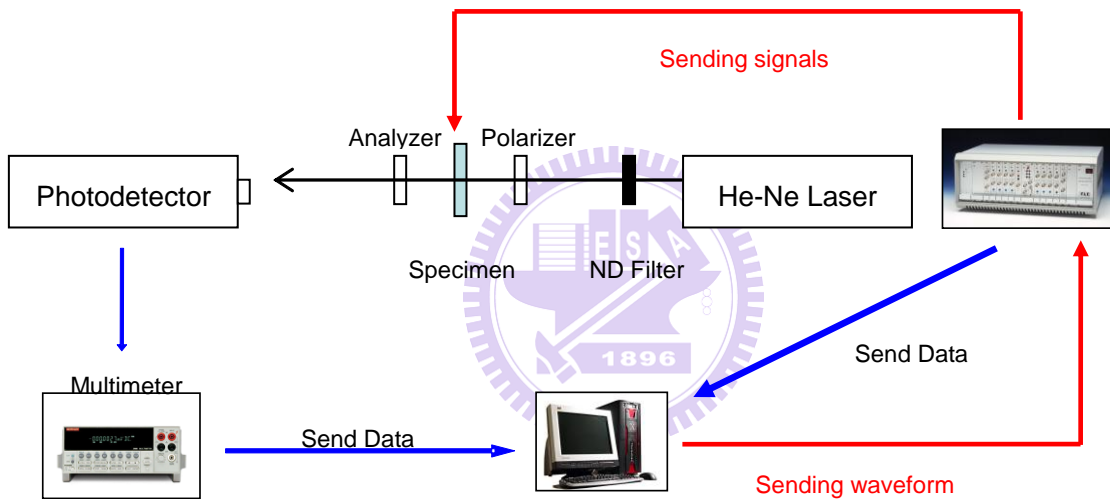


Fig. 3-4 Schematic diagram of electro-optical measurement system

3.5 Anchoring Energy Measurement

Anchoring energy is used to describe the interaction between liquid crystal molecules and the alignment layer. Anchoring energy is an important factor in liquid crystal alignment, influencing directly the electro-optical performance of TN cells. We can use anchoring energy to quantify the alignment strength and determine the

feasibility of liquid crystal alignment method. Anchoring energy can be separated into two kinds: polar anchoring energy and azimuthal anchoring energy. The strength of polar anchoring energy will affect significantly the electro-optical properties and the tilt angle of liquid crystal while the strength of azimuthal anchoring energy will influence the orientational order and the orientation of liquid crystal molecules in azimuthal direction. In general, azimuthal anchoring energy is much smaller than polar anchoring energy so it is more difficult to measure azimuthal anchoring energy. Therefore, in this research, we concentrate on the measurement of polar anchoring energy by Liquid Crystal Analysis System (LCAS). Based on the value of measured polar anchoring energy, we give an explanation for the electro-optical performances of different alignment materials.

A variety of methods were proposed to measure polar anchoring energy such as surface disclination method, Freedericksz transition method [71-72], high electric field method [73-74], and capacitance method [75]. In this thesis, we use the capacitance method to determine polar anchoring energy of various alignment materials. The principle of the capacitance method is described in detail as below.

We consider a cell filled with positive dielectric anisotropy LC and rubbed anti-parallel direction. When no electric field is applied, all LC molecules are aligned parallel to the alignment direction on the surface of alignment layer. When the applied voltage is larger than the threshold voltage, LC molecules begin to tilt. Almost LC molecules in the cell will tilt up perpendicular to the surface (along the electric field) so the capacitance of the cell will nearly be the same with an increase of applied voltage. Due to the effect of the anchoring strength of LC-surface interaction, the tilted angle of LC molecules near the surface is smaller than that in the middle of the cell. Therefore, we can observe the optical properties of LC cell put in the electric field in order to obtain the polar anchoring energy. The calculation of the polar anchoring

energy is assumed based on the elastic continuum theory.

The capacitance of LC cell is determined by the cell gap d , area of electrodes S and the dielectric permittivity of LC ϵ which is a function of the applied voltage. For the high voltage $V > 6V_{th}$, the capacitance of LC cell can be written as follow

$$C = \frac{\epsilon_0 \epsilon_{//} S}{Qd} \left(1 - \frac{\bar{V}}{V} \right) \quad (3-11)$$

$$\text{where } \bar{V} = \alpha \frac{\epsilon_a}{\epsilon_{//}} V_{th} \quad \epsilon_a = \epsilon_{//} - \epsilon_{\perp} \quad V_{th} = \pi \sqrt{\frac{K_{11}}{\epsilon_0 \epsilon_a}} \quad \alpha = \frac{1}{\pi} \int_{y_p}^1 \sqrt{\frac{(1+\gamma)(1+ky)}{y(1+\gamma y)}} dy$$

$$\gamma = \frac{(\epsilon_{//} - \epsilon_{\perp})}{\epsilon_{\perp}} \quad k = \frac{K_{33} - K_{11}}{K_{11}}$$

$$y = \sin^2 \theta \quad y_p = \sin^2 \theta_p$$

S is the electrodes overlapping square.

$\epsilon_{//}$, ϵ_{\perp} are the LC dielectric constants parallel and perpendicular to the LC director.

θ_p is pretilt angle.

K_{11} , K_{33} is the elastic constant of splay and bend state.

$$Q = 1 - \frac{2K_{11}}{Wd} \frac{\gamma(1+ky_p)(1-y_p)}{1+\gamma y_p} \quad (3-12)$$

For the small pretilt angle $\theta_p < 10^0$, we have

$$Q = 1 - \frac{2\gamma K_{11}}{Wd} \quad (3-13)$$

We can find out the polar anchoring energy W from Fig. 3-12. By determining the value of capacitance C_{inf} at high voltage $V \rightarrow \infty$, the value of threshold voltage V_{th} and using Eq. 3-11, we can obtain

$$W = \frac{2}{\pi^2} \frac{V_{th}^2}{S} \frac{(C_{//} - C_{\perp})^2}{C_{\perp}} \frac{1}{1 - C_{//}/C_{inf}} \quad (3-14)$$

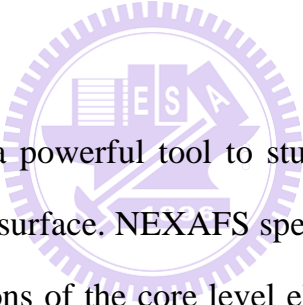
Where C_{\perp} is the capacitance of LC cell for planar orientation, can be obtained at the applied voltage smaller than the threshold voltage ($V < V_{th}$).

$C_{//}$ is the capacitance of LC cell for homeotropic orientation, can be obtained at a very high voltage.

C_{inf} is the infinitive capacitance, can be obtained by a linear approximation fit.

By substituting the value of V_{th} , S , $C_{//}$, C_{\perp} , and C_{inf} into Eq. 3-14, we can calculate the value of polar anchoring energy.

3.6 NEXAFS Measurement



NEXAFS spectroscopy is a powerful tool to study the orientation of functional groups of organic molecules on surface. NEXAFS spectra are measured by resonances absorption arising from transitions of the core level electron to unoccupied molecular orbitals of π^* and σ^* symmetries. In this research, the near-edge X-ray absorption fine structure spectra are carried out at the undulator beam line 05B2 EPU-PEEM station of National Synchrotron Radiation Research Center by using linearly polarized soft X-rays. The energy resolution was 100 meV at the Carbon K-shell absorption edge. For the NEXAFS measurements, $0.7 \times 0.7 \text{ cm}^2$ pieces cut from rubbed polymer samples are used. Polarization-dependent NEXAFS spectra are recorded for in-plane and out-of-plane asymmetries with the electric field vector in the (x,y) plane and (x,z) plane, respectively, at the fixed X-ray incident angle. Both the in-plane and out-of-plane asymmetries at the rubbed surfaces of various new alignment materials will be examined in chapter 4.

3.7 Fabrication Process

3.7.1 Flow chart

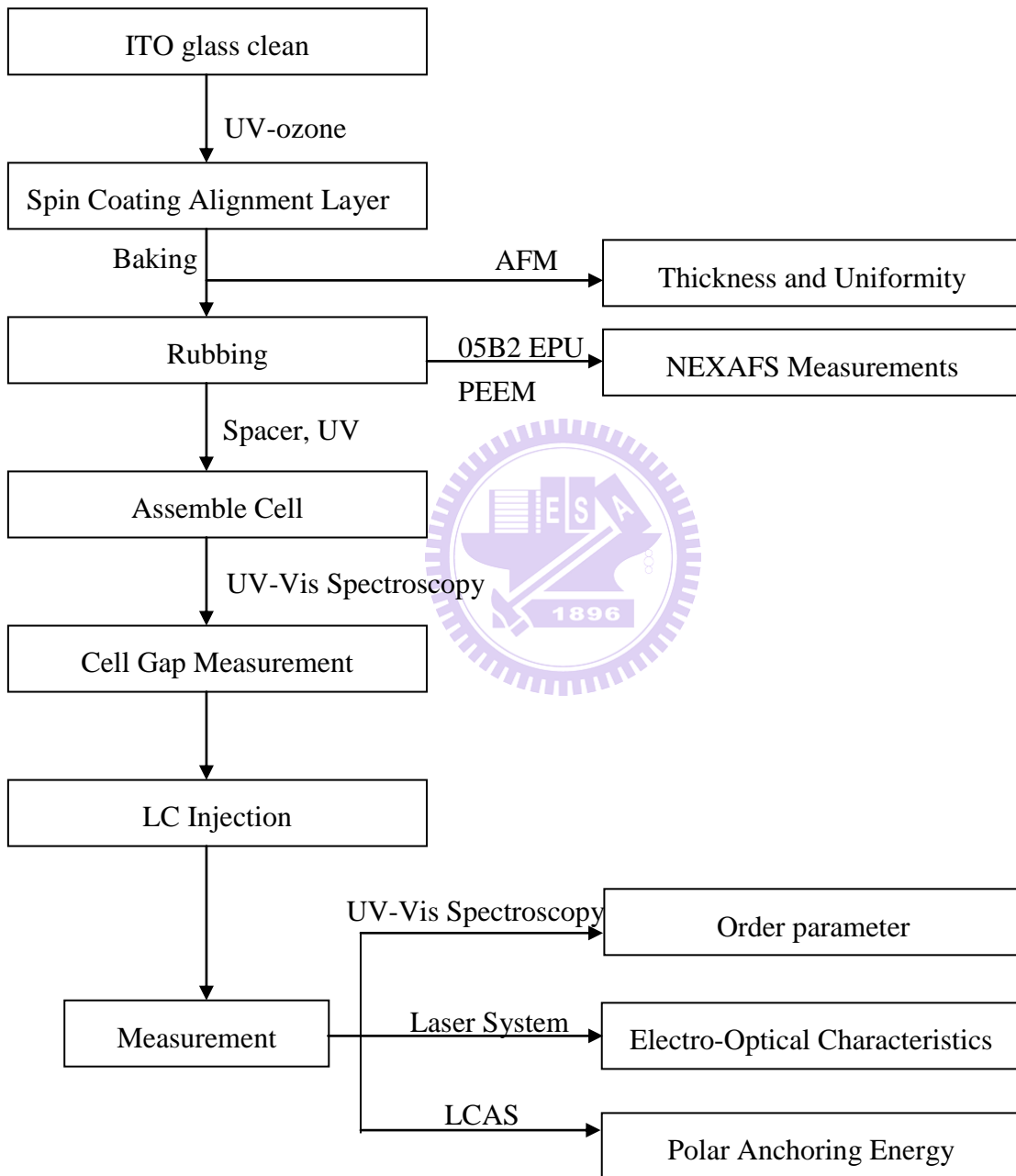


Fig. 3-5 Flow chart of fabrication process

3.7.2 Fabrication Process

1. The glass is the most common substrate used in liquid crystal display technology. The glasses with the thickness of 1.1 mm are uniformly sputtered by ITO in one side to make the conductive layers on the surface of the glasses. Small glass pieces of 2 cm x 2.5 cm are cut from the big one by the cutting machine and marked the side containing ITO.

2. Clean substrates are very essential for the quality of all devices in general and LC devices in particular. Firstly, a holder containing 20 pieces of ITO glass is rinsed by DI water for 5 minutes. Next, each piece of ITO glass is covered with detergent solution and carefully rubbed by hands. Thirdly, ITO glasses are washed with deionized (DI) water. A remarkable sign to recognize the clean ITO glasses is that DI water can flow smoothly along their surfaces. Then, the holder loads the clean ITO glasses is immersed into clean DI water for 5 minutes and in ultra sonic for 40 minutes. After that, nitrogen gas is used to blow off water from the surface of ITO glasses. Finally, these clean ITO glasses are baked at 110° C for 30 minutes to completely evaporate water on the surface.

3. In order to have better adhesion and hydrophilic of alignment layer, the surface of clean ITO glasses is treated by UV-Ozone for 30 minutes. A mixture solution is formed by mixing each material and its own solvent. The weight ratio of the mixture solution is controlled to get suitable thickness of alignment layer less than 100nm for display applications.

Clean ITO glasses are put on the truck of spin coater. The formation of uniform alignment layer on the surface of samples is processed by the following steps. Firstly, the pure solvent is drop on the whole surface of ITO glasses and spin. Secondly, these glasses are totally covered with the mixture solution and spin. Then, these samples are

baked to appropriate temperature for 1 h to remove the solvent and to relax the films. The parameters of spin coating process of alignment materials are shown in detail in Table 3-1.

Table 3-1 Specific parameters of spin coating process for solvent (top) and mixture solution (bottom)

	Time (sec)	Speed (rpm)
Solvent-waiting	5.0	0
Solvent-waiting	0.8	800
Solvent-low spin	10	800
Solvent-waiting	3.2	4000
Solvent-fast spin	20	4000
Solvent-waiting	5	0

	Time (sec)	Speed (rpm)
Mixture solution-waiting	5.0	0
Mixture solution-waiting	0.8	800
Mixture solution -low spin	30	800
Mixture solution -waiting	3.2	4000
Mixture solution -fast spin	60	4000
Mixture solution -waiting	5	0

Table 3-2 indicates specific parameters of various materials, namely, solvent of each material, the weight ratio for the mixture solution, the thickness of alignment film, and the baking temperature for each material.

Table 3-2 Specific parameters of different materials

Material	PI	PVA	PS	PSSA	PVP	PVPD
Solvent	NBC-311	Water	Toluene	Water	Pentanol	Water
Weight Ratio	50%	2.5%	0.5%	2.4%	0.5%	0.1%
Thickness	34nm	66nm	39nm	36nm	37nm	10nm
Temperature	220 ⁰ C	110 ⁰ C	150 ⁰ C	110 ⁰ C	150 ⁰ C	110 ⁰ C

4. The samples are rubbed by rubbing machine. The rubbing directions of top and bottom samples are perpendicular to each other to make a twisted nematic cell.

5. UV glue (NOA-65, from Norland) is mixed with 5% of 5.0um spacer. A small amount of above mixture is dropped at the edges of the bottom sample which is covered and uniformly pressed by the top sample, making an empty cell. Then, the empty cell is placed under a UV lamp for 5 minutes to fully cure the glue.

6. The cell gap of the empty cell is measured by UV/Vis Spectrophotometer Lambda 650 using interferometric method, is explained in detail in section 3.3.1.

7. The nematic liquid crystal (E7, from Merck) is injected into the empty cell by capillarity phenomenon, finishing a LC cell (as depicted in Fig. 3-6).

8. The ITO contact of LC cell is soldered by the wire, available for the electro-optical measurements.

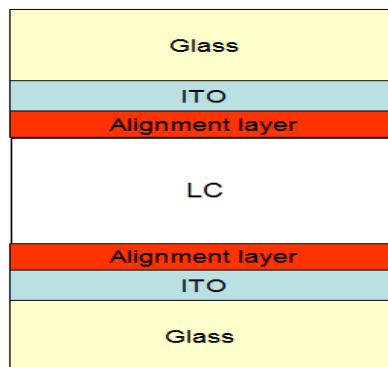


Fig. 3-6 Schematic of a liquid crystal cell

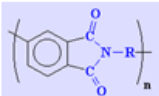
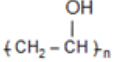
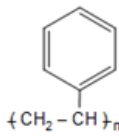
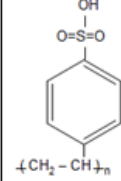
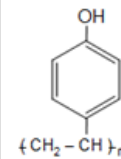
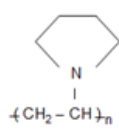
Chapter 4

Experiment Results and Discussion

4.1 Surface Morphology of Alignment Materials

In this thesis, a variety of polymers having distinct chemical functional groups are tested as new liquid crystal alignment materials, namely polystyrene sulfonic acid (Mw = 75,000 from Alfa Aesar), poly (4-vinylphenol) (Mw = 8,000 from Sigma-Aldrich), and polyvinylpyrrolidone (Mw = 40,000 from TCI). Moreover, the performances of the other alignment materials such as polyimide (PIA-X201-G01 from Chisso), polyvinyl alcohol (Mw = 13,000-23,000 from Sigma-Aldrich), and polystyrene (from Alfa Aesar) are also examined to compare with those of new alignment materials. The glass transition temperature T_g of new materials is over 150⁰ C. The chemical structures of alignment materials presented in my thesis are described in Table 4-1.

Table 4-1 Chemical structures of different materials

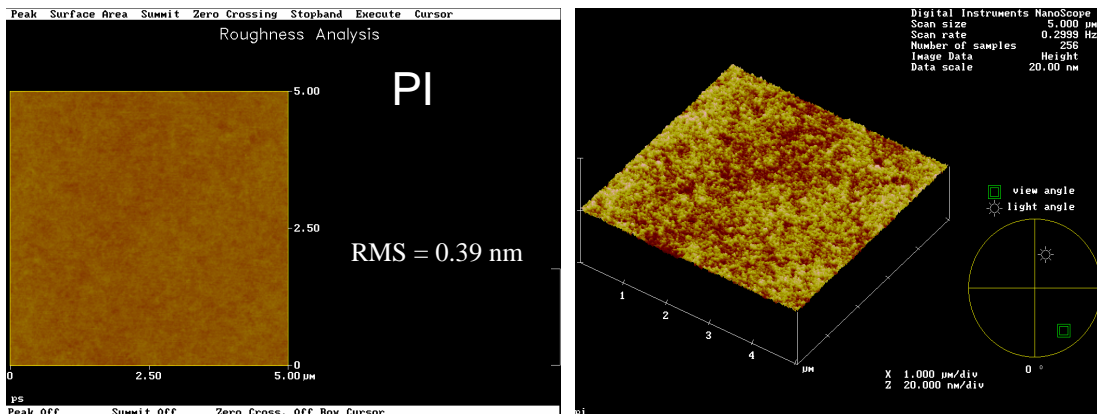
Material	PI	PVA	PS	PSSA	PVP	PVPD
Chemical structure						

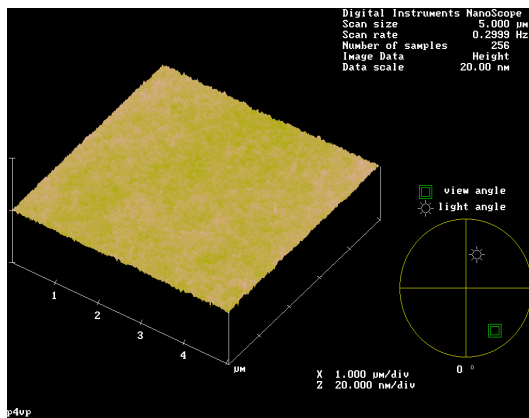
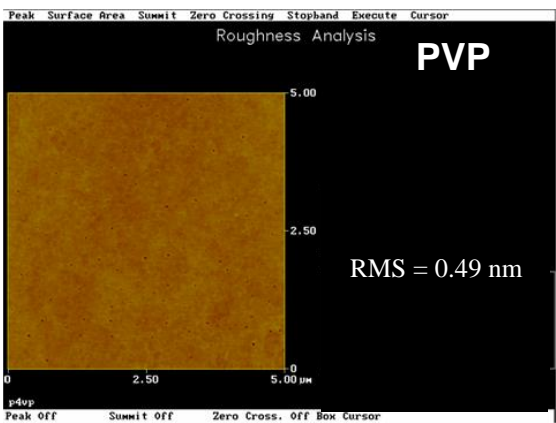
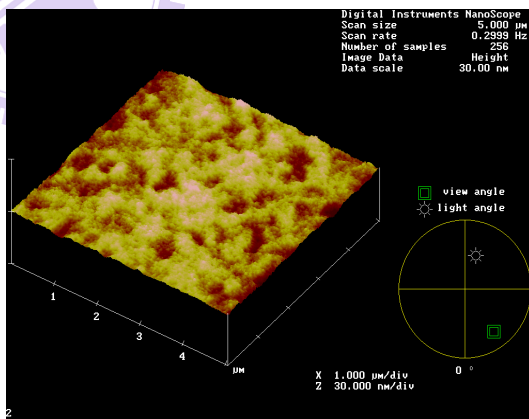
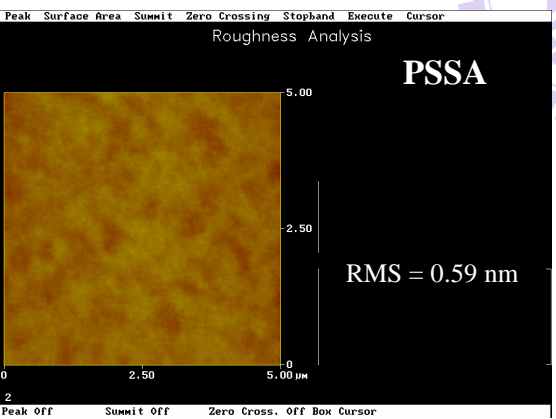
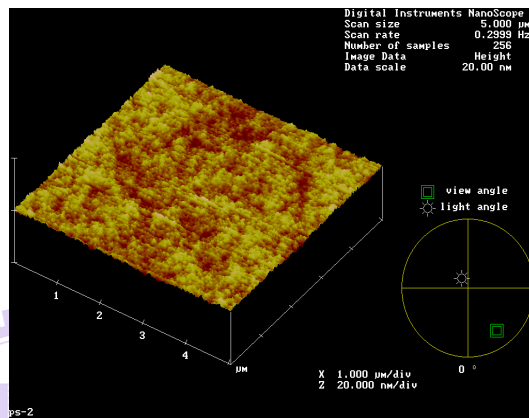
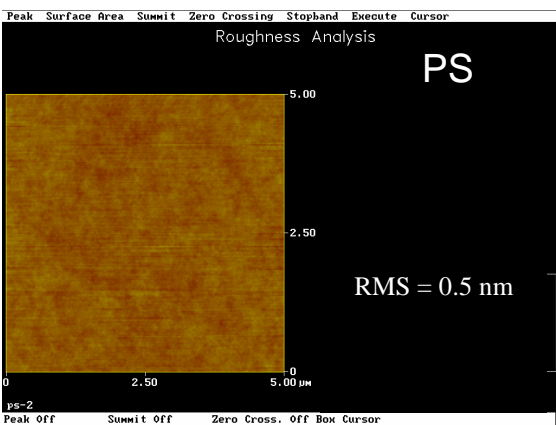
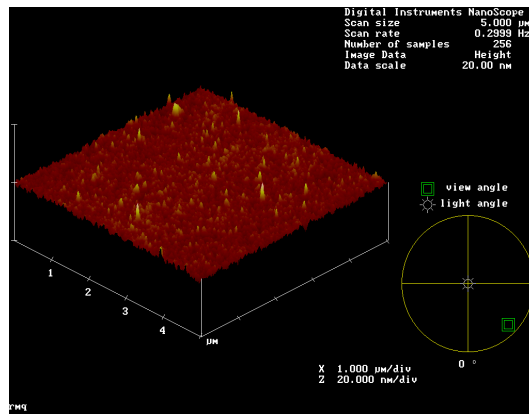
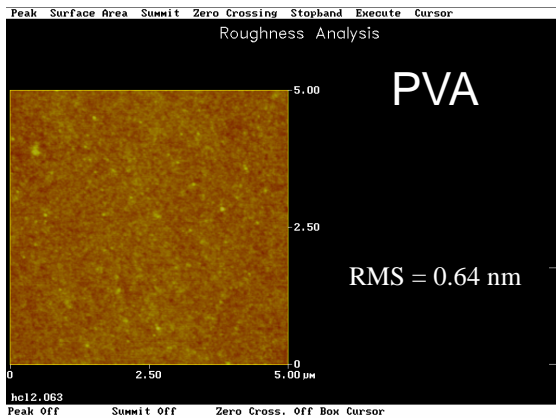
Besides the phenyl rings in side chain like PS, the prepared polymers PSSA and PVP also contain additional specific chemical functional groups, namely, HSO_3 and OH in turn. The comparison in the performances of rubbed PS, PSSA, and PVP helps us realize whether the chemical functional groups play any role in liquid crystal aligning ability.

Among these materials, PVPD is one kind of non aromatic carbonyl containing polymers, having carbonyl group in the side chain and no phenylene in the main chain [76]. Particularly, the side chain of PVPD contains carbonyl groups connected with five-sides rings rotate freely in its side chain.

Besides, PVA is one type of saturated polymers which include only single bonds in their structure. The side chain of PVA is only composed of OH groups in specific. The aligning abilities of those materials in Table 4-3 are evaluated through their whole performances.

For LCD device applications, uniform alignment of liquid crystal molecules on the surface of alignment layer is of great importance because of LC-surface direct interaction. The surface morphology of all materials presented in my thesis is observed by atomic force microscope.





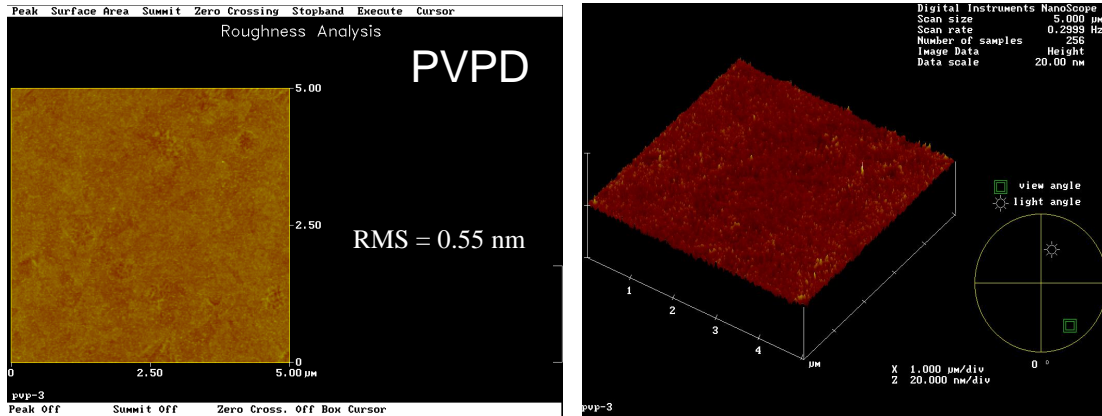


Fig. 4-1 AFM images and RMS roughness values of PI, PVA, PS, PSSA, PVP, and PVPD, respectively

The surface morphologies of all materials are measured at several different positions on their surfaces. Fig. 4-1 presents the average root mean square (RMS) roughness values of different materials, namely PI, PVA, PS, PSSA, PVP, and PVPD. RMS values of PI, PVA, PS, PSSA, PVP, and PVPD are 0.39nm, 0.64nm, 0.5nm, 0.59nm, 0.49nm, and 0.55nm, respectively. Uniform surfaces with root mean square roughness values less than 1 nm can be achieved by all of these materials. The uniformity of surface is a prerequisite requirement for alignment materials before their other performances are continuously examined, for example, electro-optical characteristics, order parameter, polar anchoring energy, and NEXAFS measurements for evaluating their overall aligning ability.

4.2 Order parameter

The order parameter which describes the orientational order of liquid crystalline materials is also quantified. To measure the order parameter of different alignment materials, the anti-parallel cells are prepared and filled with the mixture of nematic LC E7 and 2% dye S428. The calculation for determining the value of order parameter for each alignment material is mentioned in the section 3.3.2. The order parameter of different alignment materials are obtained at the wavelength of 645nm of absorption spectra. Table 4-2 lists the values of order parameter of various alignment materials treated by mechanical rubbing method.

Table 4-2 Order parameters of different rubbed polymers

Material	PI	PVA	PS	PSSA	PVP	PVPD
Order parameter	0.6	0.59	0.3	0.5	0.5	0.48

Among these alignment materials, only rubbed PS shows a very low order parameter value of 0.3. The values of order parameter of rubbed PSSA, PVP, and PVPD are 0.5, 0.5, and 0.48, respectively, being able to compare with those of rubbed PI and rubbed PVA which are 0.6 and 0.59, respectively. The higher the order parameter is, the better the aligning ability is. In terms of order parameter, rubbed PVPD shows absolute success.

4.3 Electro-optical characteristics of TN cells

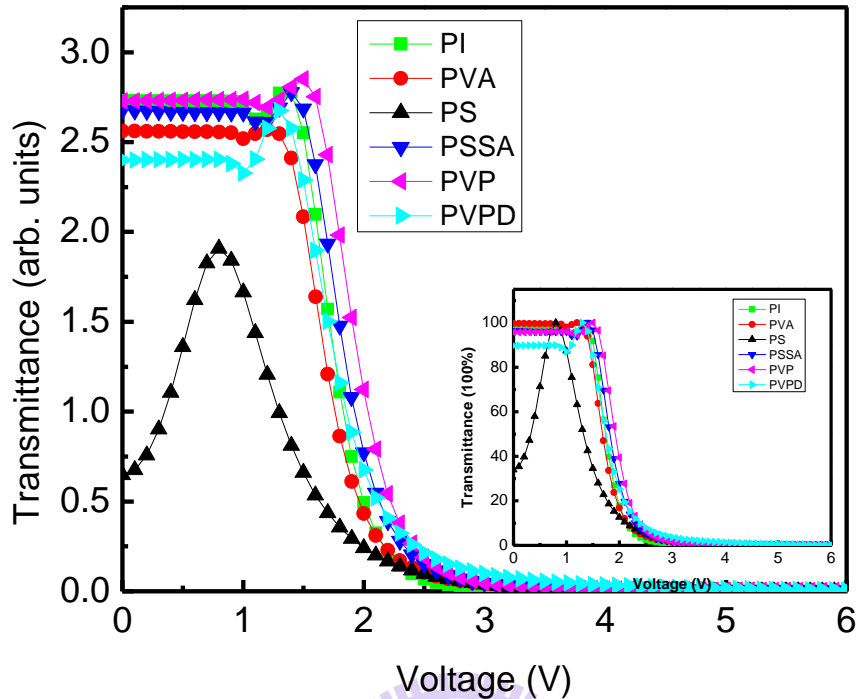


Fig. 4-2 V-T curves of TN cells using rubbed PI, PVA, PS, PSSA, PVP, and PVPD, respectively. The inset shows the normalized V-T curves

Besides the order parameter, the performances of various alignment materials are investigated in terms of their electro-optical properties. The voltage-transmittance (V-T) curves of the TN cells fabricated on different rubbed polymer surfaces are studied to examine the application potential of liquid crystal alignment materials. Fig. 4-2 shows the optical transmittance governed by the aligning ability of new materials induced by rubbing method, including rubbed PSSA, rubbed PVP, and rubbed PVPD in the comparison with rubbed PI, rubbed PVA, and rubbed PVPD. The V-T curves have small bumps in the threshold regions, resulting from the large retardation value of the cells over the first maximum condition of 0.48mm for normally white TN cells [77-79]. In general, the maximum light transmittances of TN cells of rubbed PSSA, rubbed PVP, and rubbed PVPD are comparable with those of rubbed PI and PVA, except for the case of rubbed PS. Poor electro-optical properties of rubbed PS can be

explained due to its weak aligning ability [31] as well as its weak anchoring energy [35, 80]. A comparison in terms of electro-optical properties of rubbed PS, PSSA, and PVP proves the importance of functional groups of rubbed polymer surfaces in orienting LC molecules. Among new materials, the electro-optical properties of rubbed PVPD are found to be not as stable as those of rubbed PSSA and PVP. Only about 70% in the total amount of TN cells fabricated with rubbed PVPD succeed in obtaining good V-T characteristics while good V-T curves fabricated with rubbed PSSA and PVP are obtained absolutely, maybe due to its weak anchoring energy. The anchoring energy of new materials will be measured later.

Table 4-3 Specific parameters of V-T curves using different rubbed surfaces

Material	V_{th}	V_{sat}
PI	1.5	2.14
PVA	1.43	2.17
PSSA	1.56	2.3
PVP	1.65	2.37
PVPD	1.68	2.39

Table 4-3 depicts specific parameters of electro-optical characteristics measured from different rubbed polymer surfaces such as threshold voltage (V_{th}), saturation voltage (V_{sat}). Threshold voltage is defined as root mean square voltage value at which light transmission has changed 10% of the maximum light transmittance value. Saturation voltage is defined as root mean square voltage value at which light transmission has changed 90% of the maximum light transmittance value.

The threshold voltages of rubbed PSSA, PVP, and PVPD layers are 1.56 V, 1.65 V, and 1.68 V, respectively, while those of rubbed PI and PVA layers are 1.5 V

and 1.43 V. Furthermore, the saturation voltages of rubbed PSSA, PVP and PVPD are 2.3 V, 2.37 V, and 2.39 V, respectively, while those of rubbed PI and PVA are 2.14 V and 2.17 V. The threshold and saturation voltages of rubbed PSSA, PVP, and PVPD show a small difference in the range of 0.2 V compared to those of rubbed PI and PVA. Therefore, the electro-optical performances of new materials induced by rubbing treatment are comparable with those of rubbed PI and PVA [22].

4.4 Polar anchoring energy

The physical properties at the boundary between alignment layer and liquid crystal are of great impact to the performances of LC devices. Polar anchoring energy is one of the significant factors directly influences the electro-optic characteristics of TN cells.

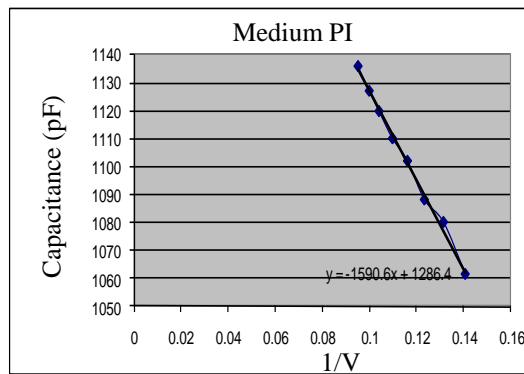
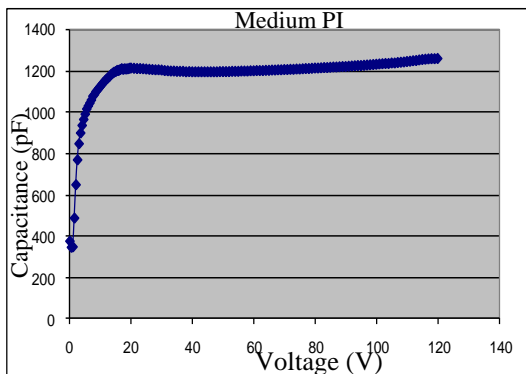
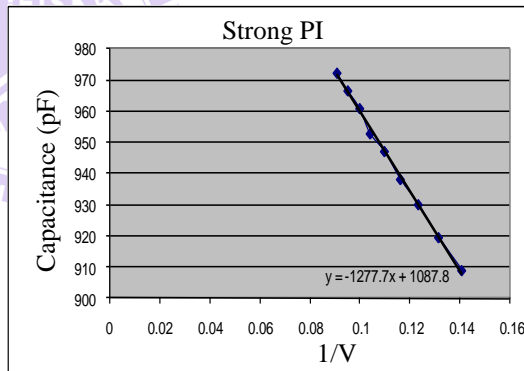
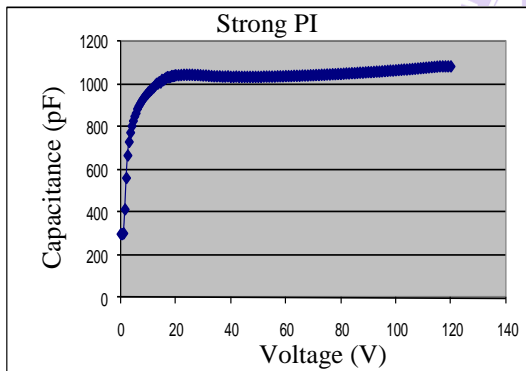
Patterned ITO glasses are used as substrates for polar anchoring energy measurement. The area of electrode is 1 cm^2 . The alignment directions of two substrates are anti-parallel and the cell gap is around $10 \mu \text{ m}$. Nematic LC (Merck MJ 051989) is injected into the empty anti-parallel cells. Liquid crystal analysis system is used to measure the polar anchoring energy based on the capacitance method and Eq. 3-14 in the section 3.5 is used for the calculation of the polar anchoring energy. We determine the polar anchoring energy at different rubbing strength conditions for various alignment materials and elucidate the electro-optical properties of TN cells affected by the anchoring energy.

We measure the polar anchoring energy for polyimide at three different rubbing strength conditions, as described in Table 4.4. N is the number of rubbings, M is the pile impression (mm), n is the rotation speed of the roller (s^{-1}), V is the advancing speed of the substrate (mm/s). The magnitude of rubbing strength is referred in the

section 2.1.1.

Table 4.4 Rubbing parameters at three different rubbing conditions

	Strong rubbing	Medium rubbing	Weak rubbing
N	5	1	1
M	0.2 mm	0.2 mm	0.2 mm
n	8.3rpm/s	8.3rpm/s	0.83rpm/s
V	7.3mm/s	7.3mm/s	10.95mm/s
Rubbing Strength	159.66mm	31.93mm	1.94mm



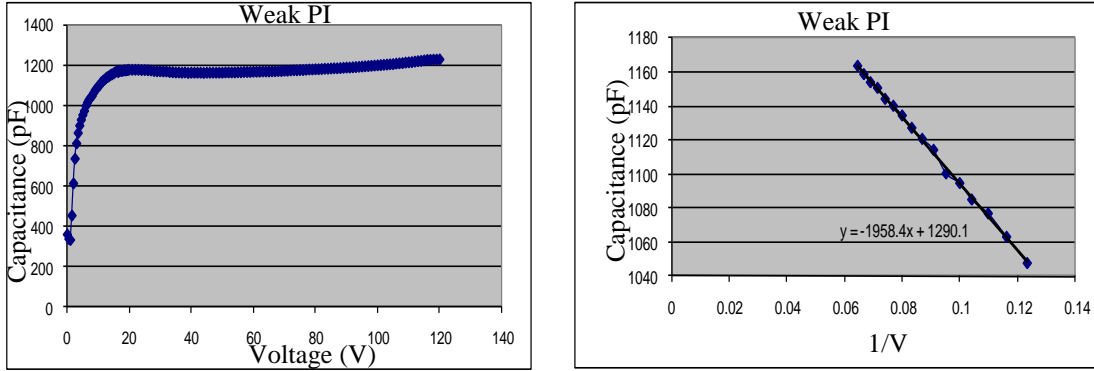


Fig. 4-3 Capacitance dependence on applied voltage for polyimide at strong, medium, and weak rubbing conditions, respectively

The values of C_{\perp} , $C_{//}$ and C_{inf} can be obtained from Fig. 4-3. In this experiment, the electrode area S is 0.0001 m^2 . The parameters for determining the polar anchoring energy of polyimide from Eq. 3-14 are listed in detail in Table 4-5.

Table 4-5 Necessary parameters for determining polar anchoring energy of polyimide at different rubbing strength conditions

	$V_{th}(V)$	C_{\perp} (pF)	$C_{//}$ (pF)	C_{inf} (pF)	W (J/m^2)
Strong PI	1.1	299.3	1082.7	1087.8	1.07×10^{-3}
Medium PI	1.1	348.6	1262.4	1286.4	3.15×10^{-4}
Weak PI	1.1	339.7	1228.1	1290.1	1.19×10^{-4}

The values of polar anchoring energy for polyimide at strong, medium, and weak rubbing are $1.07 \times 10^{-3} \text{ J/m}^2$, $3.15 \times 10^{-4} \text{ J/m}^2$, $1.19 \times 10^{-4} \text{ J/m}^2$, respectively. There is a considerable difference of an order in the magnitude of polar anchoring energy for polyimide at strong and medium rubbing conditions. The larger value of polar anchoring energy can enhance the electro-optical performance. The electro-optical

property of polyimide at strong rubbing strength shows lower threshold and saturation voltages of 0.21 V and 0.36 V compared to those at medium rubbing strength, as illustrated in Fig. 4-4. Weak rubbing strength causes poor performance of V-T curve of polyimide. In general, rubbed PI is one kind of strong polar anchoring energy, as known in literature [22, 35, 75].

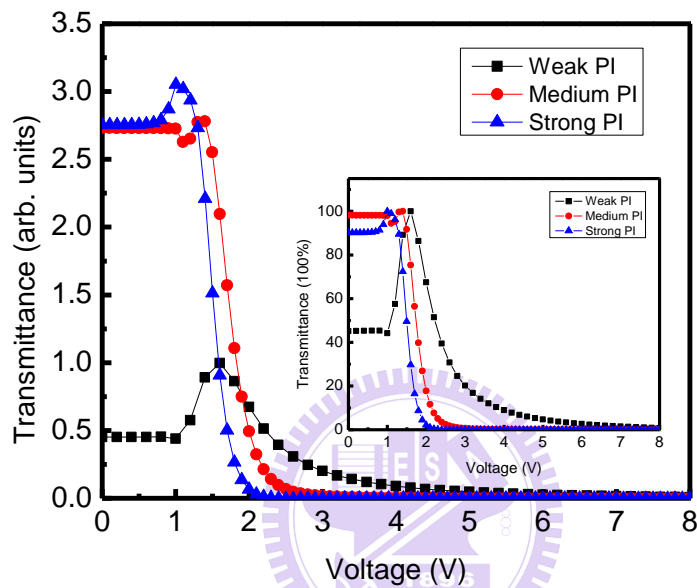


Fig. 4-4 Electro-optical properties of TN cells using rubbed PI at weak, medium, and strong rubbing strengths. The inset shows normalized V-T curves

Fig. 4-5 indicates the specific values of C_{\perp} , $C_{//}$ and C_{inf} for rubbed PSSA at different rubbing strengths. In contrast with rubbed PI, there is no considerable difference in the values of polar anchoring energy for rubbed PSSA at strong and medium rubbing conditions, which are $2.65 \times 10^{-4} \text{ J/m}^2$ and $1.08 \times 10^{-4} \text{ J/m}^2$, respectively, as obtained in Table 4-6.

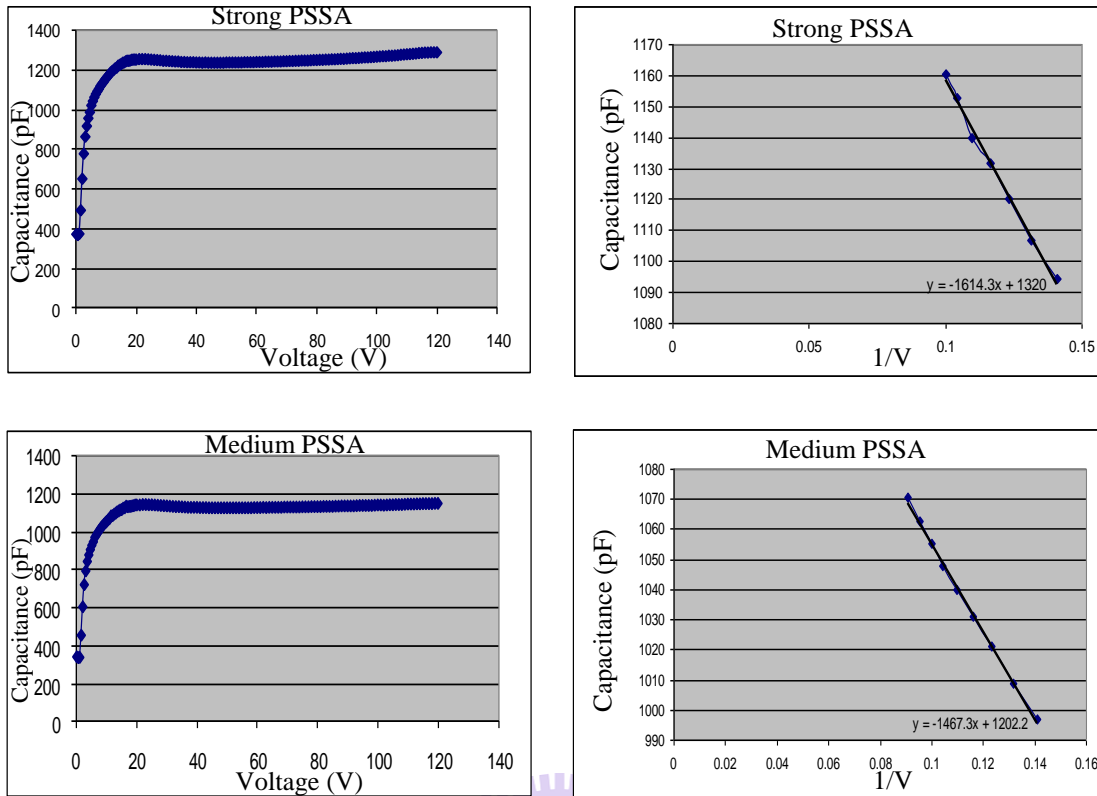


Fig. 4-5 Capacitance dependence on applied voltage for PSSA at strong (top) and medium (bottom) rubbing conditions

Table 4-6 Necessary parameters for determining polar anchoring energy of PSSA at different rubbing strength conditions

	$V_{th}(V)$	C_{\perp} (pF)	$C_{//}$ (pF)	C_{inf} (pF)	W (J/m^2)
Strong PSSA	1.1	366.1	1291.4	1087.8	2.65×10^{-4}
Medium PSSA	1.1	340.3	1149.8	1202.2	1.08×10^{-4}

The comparison of V-T curve for rubbed PSSA at strong and medium rubbing strengths is described in Fig. 4-6. There is a slight shift of 0.12 V and 0.25 V in the values of threshold and saturation voltages of rubbed PSSA at these two rubbing conditions. Generally, we can suppose that PSSA induced by rubbing treatment is one kind of medium polar anchoring energy (on the order of 10^{-4}).

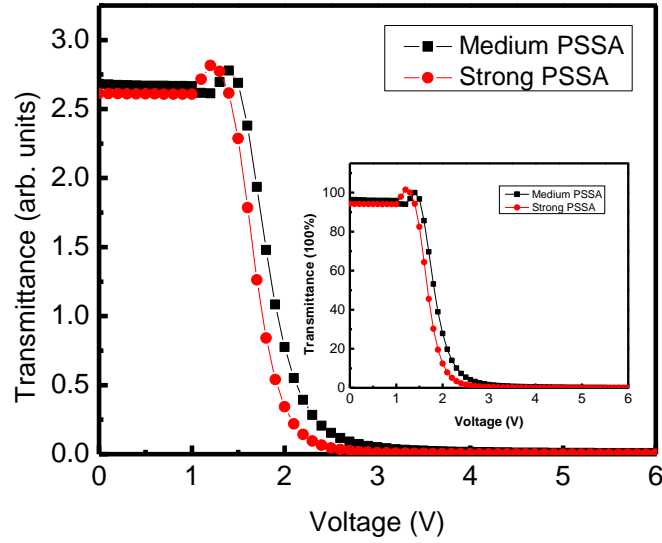


Fig. 4-6 Electro-optical properties of TN cells using rubbed PSSA at medium and strong rubbing strengths. The inset shows the normalized V-T curves

Capacitance dependence as a function of applied voltage and the linear fit curve supply the values of C_{\perp} , $C_{//}$ and C_{inf} for rubbed PVP, as observed in Fig. 4-7. In the case of rubbed PVP, the values of polar anchoring energy at strong and medium rubbing strengths are $5.46 \times 10^{-4} \text{ J/m}^2$ and $1.99 \times 10^{-4} \text{ J/m}^2$ in turn, as observed in Table 4-7. Despite of being rubbed at strong rubbing condition, there is only a small increase in the value of polar anchoring energy at strong rubbing condition.

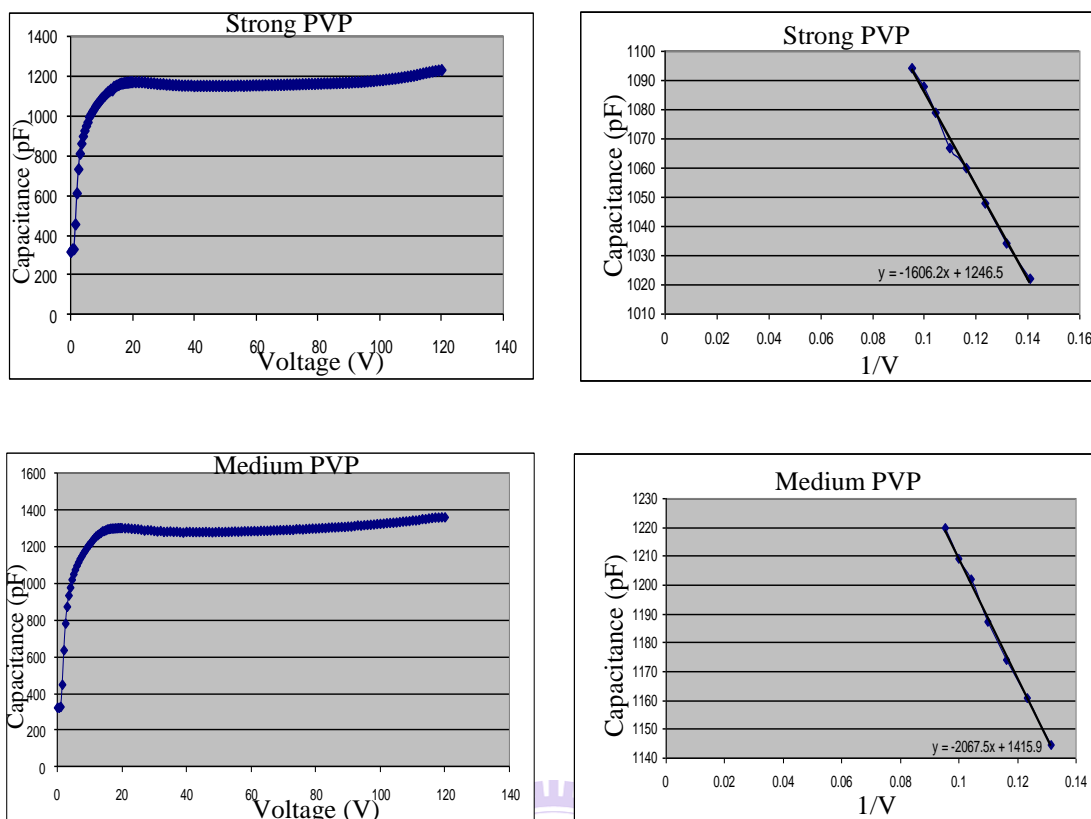


Fig. 4-7 Capacitance dependence on applied voltage for PVP at strong (top) and medium (bottom) rubbing conditions

Table 4-7 Necessary parameters for determining polar anchoring energy of PVP at different rubbing strength conditions

	$V_{th}(V)$	C_{\perp} (pF)	$C_{//}$ (pF)	C_{inf} (pF)	W (J/m^2)
Strong PVP	1.1	366.1	1291.4	1087.8	5.46×10^{-4}
Medium PVP	1.1	340.3	1149.8	1202.2	1.99×10^{-4}

The increase of polar anchoring energy can result in a better performance of electro-optical properties of rubbed PVP at strong rubbing strength, as observed in Fig. 4-8. The threshold and saturation voltages of rubbed PVP at strong rubbing strength are lower in the magnitude of 0.26 V and 0.29 V, respectively, than those at medium

rubbing strength. Although the V-T characteristics are improved, the values of polar anchoring energy at these two rubbing conditions are on the order of 10^{-4} in general. Therefore, it can be suggested that rubbed PVP has medium polar anchoring energy (on the order of 10^{-4}).

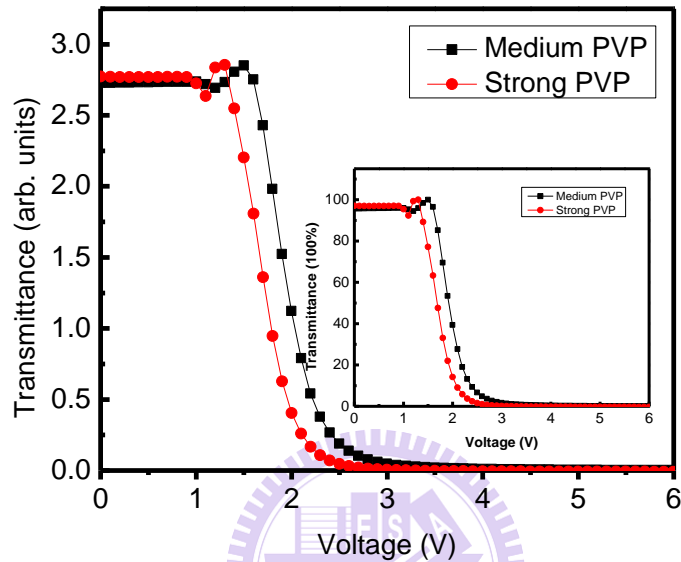


Fig. 4-8 Electro-optical properties of TN cells using rubbed PVP at medium and strong rubbing strengths. The inset shows the normalized V-T curves

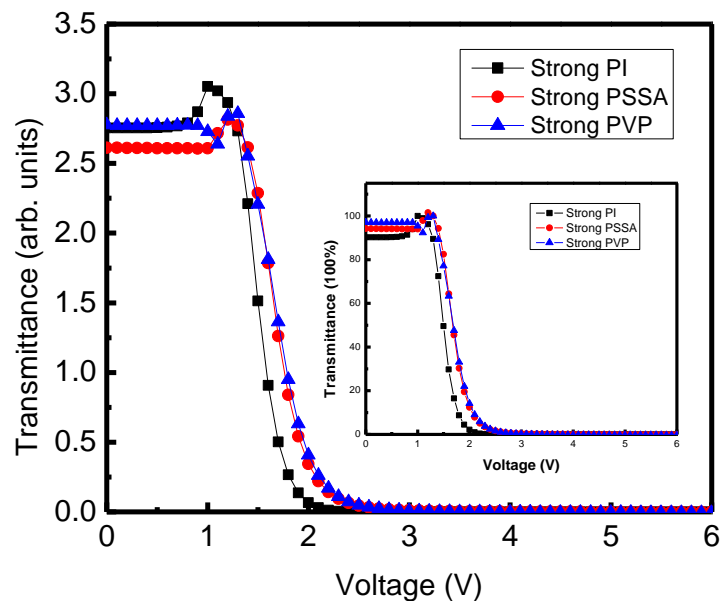


Fig. 4-9 Electro-optical properties of TN cells using rubbed PI, PSSA, and PVP at strong rubbing strength. The inset shows the normalized V-T curves

Fig. 4-9 illustrates V-T curves made from rubbed PI, PSSA, and PVP at strong rubbing strength. Weaker polar anchoring energy of rubbed PSSA and PVP can result in their electro-optical characteristics are not really as perfect as those of rubbed PI. Besides, the transmittance property and order parameter (as observed in Table 4-8) are almost identical for both rubbed PSSA and PVP layers.

Table 4-8 Order parameters of rubbed PI, PSSA, and PVP at strong rubbing strength

	Strong PI	Strong PSSA	Strong PVP
Order parameter	0.6	0.55	0.57

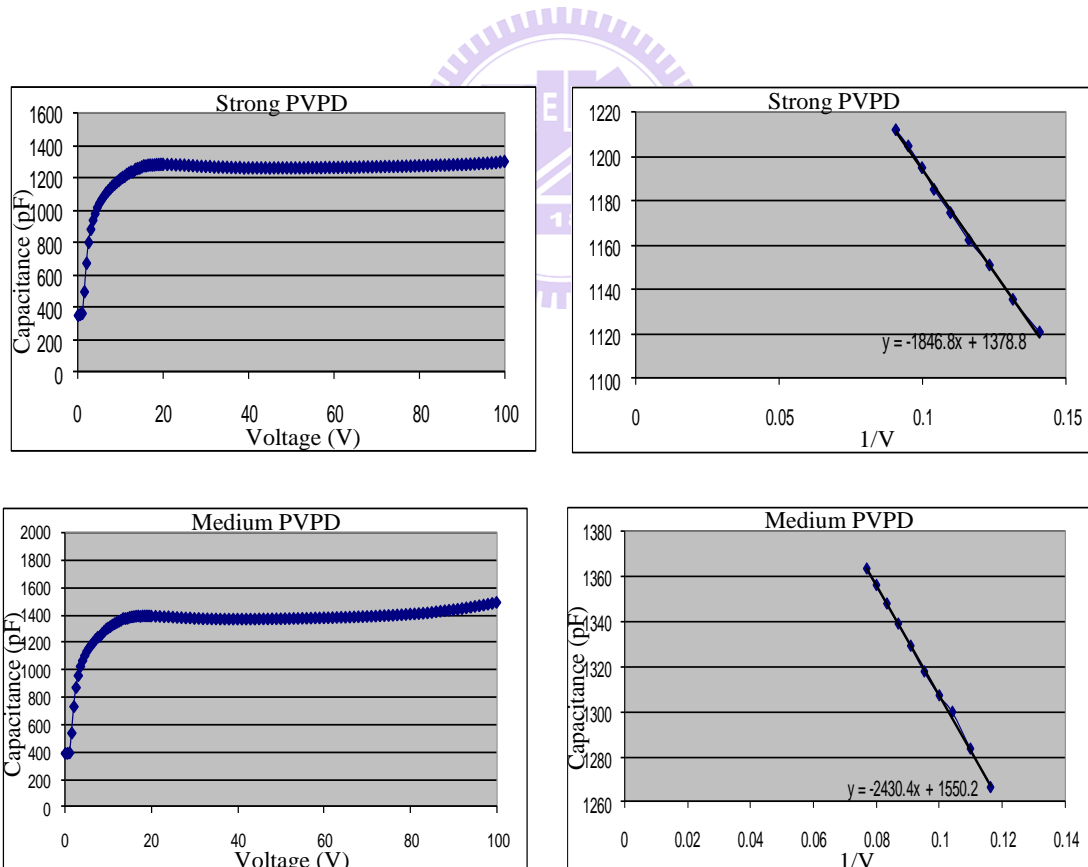


Fig. 4-10 Capacitance dependence on applied voltage for PVPD at strong (top) and medium (bottom) rubbing conditions

Table 4-9 Necessary parameters for determining polar anchoring energy of PVPD at different rubbing strength conditions

	$V_{th}(V)$	$C_{\perp} (pF)$	$C_{//} (pF)$	$C_{inf} (pF)$	$W (J/m^2)$
Strong PVPD	1.1	352.4	1285.5	1378.8	8.96×10^{-5}
Medium PVPD	1.1	391.9	1385.6	1550.2	5.82×10^{-5}

Similarly, the values of polar anchoring energy for PVPD at strong and medium rubbing strengths are $8.96 \times 10^{-5} J/m^2$ and $5.82 \times 10^{-5} J/m^2$, as seen in Fig. 4-10 and Table. 4-9. Therefore, rubbed PVPD is considered as one type of weak polar anchoring energy. Besides, rubbed PS is also known as one kind of weak polar anchoring energy [35, 80].

Overall, the polar anchoring energy affects V-T properties. A better performance in terms of electro-optical characteristics is found at larger values of polar anchoring energy. In general, rubbed PI has strong polar anchoring energy (on the order of 10^{-3}). Rubbed PSSA and PVP are kinds of medium polar anchoring energy (on the order of 10^{-4}). Rubbed PVPD and PS are types of weak polar anchoring energy (on the order of 10^{-5}).

4.5 NEXAFS measurements

The experimental geometries of in-plane and out-of-plane asymmetries are described in Fig. 4-11.

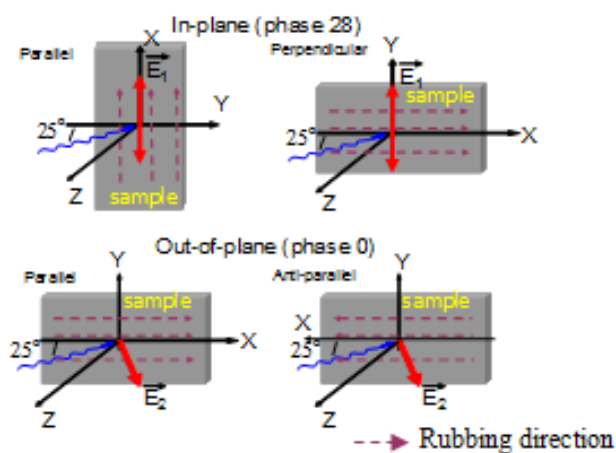


Fig. 4-11 Experimental geometries of in-plane and out-of-plane asymmetries used for the NEXAFS measurements

The rubbing direction is defined as x axis. For in-plane asymmetry, NEXAFS spectra are recorded as the direction of electric field vector E parallel to sample surface, particularly, parallel and perpendicular to the rubbing direction of sample, denoted as $E//x$ and $E//y$, respectively. For out-of-plane asymmetry, NEXAFS spectra are obtained when the direction of electric field vector E is in the plane of (x,z) and $(-x,z)$ which is parallel or antiparallel to the rubbing direction. The in-plane and out-of-plane preferential bonding orientation of each alignment material are studied in detail.

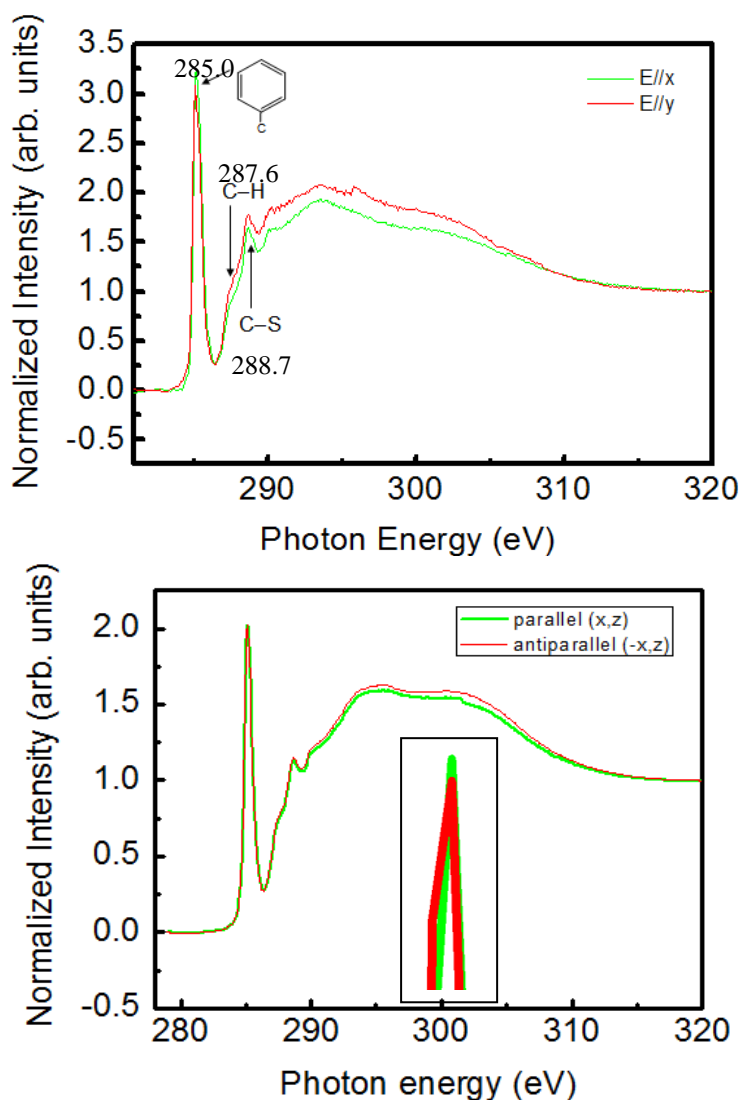


Fig. 4-12 Polarization-dependent C K-edge NEXAFS spectra of rubbed PSSA for in-plane asymmetry (top) and out-of-plane asymmetry (bottom).

Inset shows the magnification of π orbitals.

In Fig. 4-12, the in-plane and out-of plane asymmetries of rubbed PSSA are clearly illustrated. The normalized intensity of the phenyl π resonance is around 285 eV. The absorption peaks at 287.6 eV and 288.7 eV originate from the transition of C 1s to σ^* in C-H and C-S single bonds. The spectra show remarkable polarization dependence. When the electric field E vector is parallel to the normal of phenyl ring, the electron yield of π^* resonance is increased, for example, more intense peak in

spectra. The π resonance intensity is higher along x than y direction for in-plane asymmetry of rubbed PSSA which is opposite to that of all rubbed polyimides [32-34]. For out-of-plane asymmetry, the larger π intensity for (x,z) plane than (-x,z) plane is also observed. Thus, we can conclude that rubbing PSSA leads to a larger number of phenyl rings with π orbitals along x than y direction and more π orbitals are preferentially tilted from the +x axis towards the z axis, as shown in Fig. 4-13. Besides, liquid crystal molecules are oriented with their long axis perpendicular to the preferred direction of π orbitals of phenyl rings (x direction) [32-33]. As a result, liquid crystalline molecules align along y direction, meaning LCs align perpendicular to the rubbing direction. This kind of behavior of rubbed PSSA is completely opposite to that of all rubbed polyimides where LCs always orient along the rubbing direction.

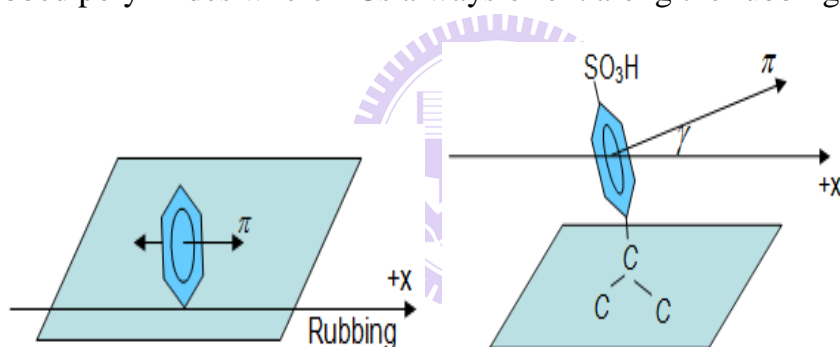


Fig. 4-13 Illustration of in-plane phenyl ring orientation (left) and a preferential tilt of phenyl planes by an angle γ from the z axis (right) of PSSA

Rubbed PS surface reveals the same behavior compared with rubbed PSSA layer for both in-plane asymmetry and out-of-plane asymmetry (as depicted in Fig. 4-14) [33]. In the NEXAFS spectra of rubbed PS, the π^* resonances corresponding to C=C double bonds in phenyl rings are labeled at the intensity of 285.2 eV and 288.0 eV, while the C-H single bond is identified at 287.3 eV.

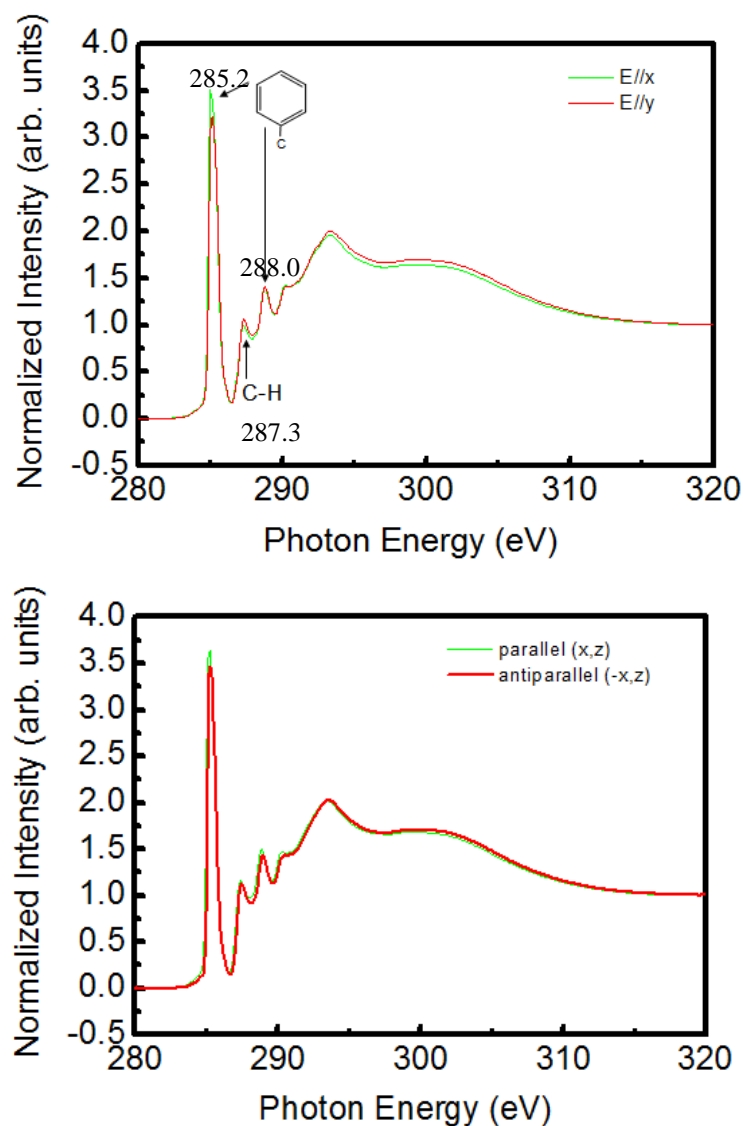


Fig. 4-14 Polarization-dependent C K-edge NEXAFS spectra of rubbed PS for in-plane asymmetry (top) and out-of-plane asymmetry (bottom)

In the case of rubbed PVP, the two sharp peaks at 285.0 eV and 287.0 eV arise from the $1s-\pi^*$ transition (C=C double bonds in phenyl ring), as observed in Fig. 4-15. Other broad peaks at higher energies come from the $1s-\sigma^*$ transition. The in-plane asymmetry of rubbed PVP presents the similar trend with that of rubbed PSSA, more phenyl rings with their π orbitals along x than y direction. The out-of-plane asymmetry, by contrast, shows the preferential tilt of π orbitals from

the $-x$ axis toward the z axis whose behavior is opposite to that of rubbed PSSA and PS. Similarly, the long axes of LCs are oriented perpendicular to the preferred direction of π orbitals of phenyl rings (x direction). Hence, the alignment directions of LCs on rubbed PVP surface are along y direction, meaning LCs orient perpendicular to the rubbing direction.

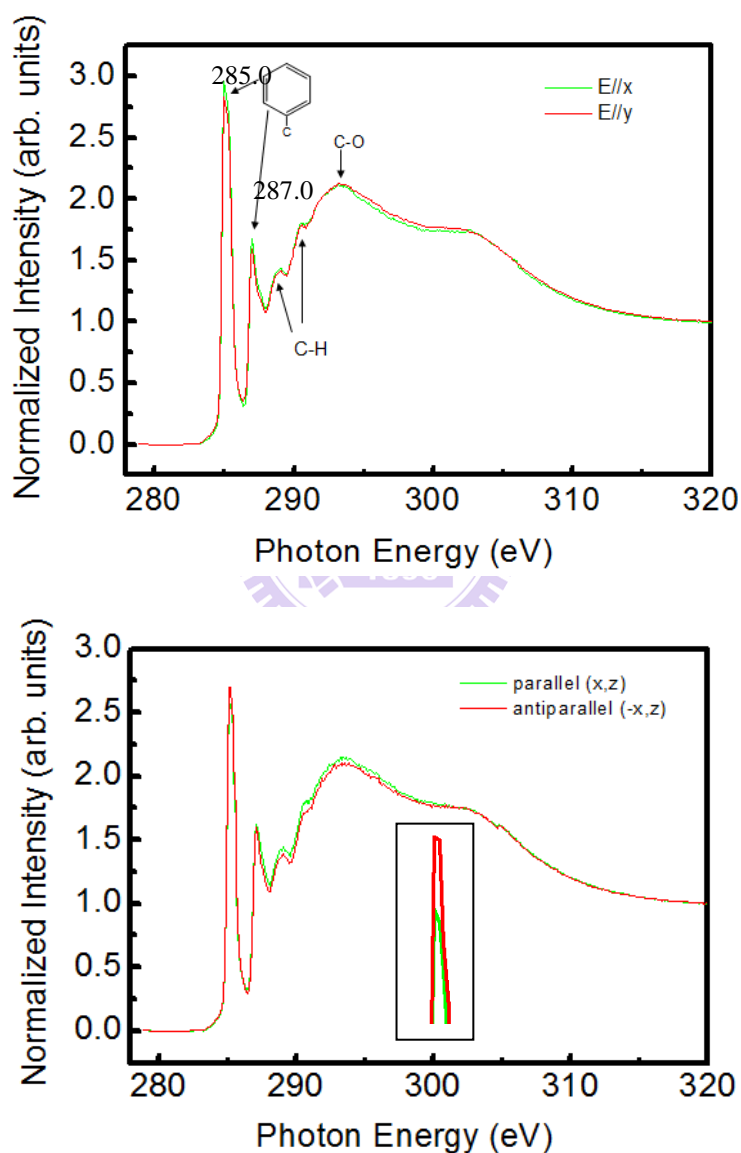


Fig. 4-15 Polarization-dependent C K-edge NEXAFS spectra of rubbed PVP for in-plane asymmetry (top) and out-of-plane asymmetry (bottom).

Inset shows the magnification of π orbitals.

The schematic orientations of phenyl ring are indicated in Fig. 4-16. The differences in the performance of aligning ability induced by rubbing treatment for PS, PSSA and PVP materials can be due to their different chemical functional groups. Therefore, the chemical functional groups play very significant roles to the LC orientation ability of alignment materials. Based on NEXAFS spectra of rubbed PSSA and PVP, we can realize that the difference between HSO_3 and OH groups is their opposite preferential tilt direction. The out-of-plane tilt direction of rubbed polymer is solely determined by the structural asymmetry at its own surface [32-33]. It can be thought that the asymmetric out-of-plane surface tilt angle depends on the nature of rubbed material. Thus, the opposite preferential tilt direction between HSO_3 and OH groups can be explained due to their different nature at rubbed surfaces.

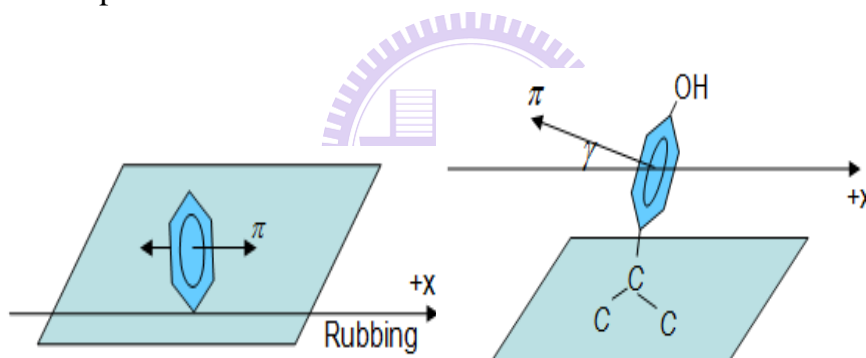


Fig. 4-16 Illustration of phenyl ring orientation (left) and a preferential tilt of phenyl planes by an angle γ from the z axis (right) of PVP.

The NEXAFS spectra of rubbed PVPD contain the sharp peak at 288.3 eV which is from C=O double bond, as shown in Fig. 4-17. Rubbing treatment induced PVPD results in more C=O groups with their π orbitals along y than x direction. Liquid crystal molecules are oriented with their long axis perpendicular to the preferred direction of π orbitals of C=O groups [33]. As a result, long axis of liquid crystal molecules are oriented perpendicular to the preferred direction of π orbitals of C=O

groups (y direction). Hence, liquid crystal molecules align along x direction, meaning LCs align parallel to the rubbing direction. This kind of behavior of rubbed PVPD is identical to that of all rubbed PI.

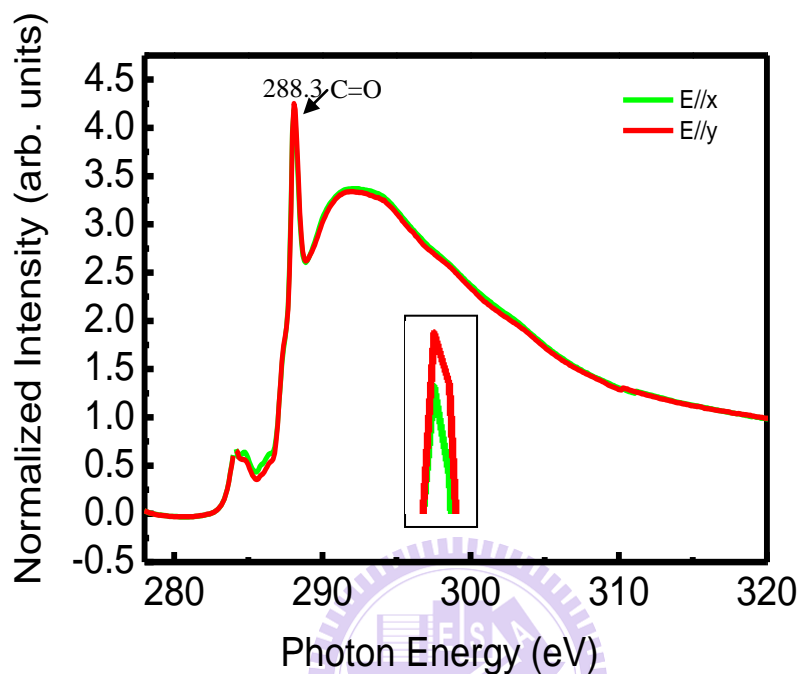


Fig. 4-17 Polarization-dependent C K-edge NEXAFS spectra of rubbed PVPD for in-plane asymmetry. Inset shows the magnification of π orbitals.

Overall, the preferential orientational distributions of liquid crystal molecules on rubbed polymer surfaces are obviously illustrated through in-plane and out-of-plane asymmetries of NEXAFS spectra. In general, rubbed PSSA, PVP, and PS align LCs perpendicular to the rubbing direction, by contrast, LCs are preferentially oriented parallel to the rubbing direction in the case of rubbed PVPD, PI, and PVA.

Chapter 5

CONCLUSIONS

5.1 Conclusions

Liquid crystal alignment layer is an important element influencing the quality and reliable of LCD. Moreover, alignment technologies determine the molecular orientation on surfaces of alignment layer. Mechanical rubbing treatment has dominated to induce the uniform orientation of liquid crystal molecules on rubbed polymer surfaces although this alignment process causes some drawbacks. Polyimide induced by rubbing treatment has dominated in the market of LCD industry. However, a major disadvantage of polyimide is its baking temperature over 200⁰ C, which restricts seriously its applications into flexible substrates. A variety of new materials containing distinct chemical functional groups such as PSSA, PVP, and PVPD tested as alignment layers for low temperature process are studied in this thesis. The temperature process of these new materials can be as low as 110⁰ C. The aligning abilities of these new materials were investigated through their performances, namely the electro-optical characteristics, the order parameter, the polar anchoring energy, and NEXAFS measurements. Furthermore, rubbed PI, PVA, and PS layers are also examined to compare their performances with those of new materials.

Among PSSA, PVP, and PS, the performances of rubbed PSSA and PVP reveal clearly better aligning abilities than those of rubbed PS. This demonstrates chemical functional groups are very significant to the aligning ability of alignment materials. Macroscopically, the HSO₃ and OH functional groups in PSSA and PVP structures, respectively, do not show big differences in their performances such as V-T curve,

order parameter, polar anchoring energy, and the in-plane asymmetry of NEXAFS spectra. Microscopically, the opposite preferential tilt direction is the only difference between these two functional groups based on NEXAFS spectra, is determined by the structural asymmetry at rubbed polymer surfaces. In general, we can suppose that HSO₃ and OH groups show the same performance.

The preferential bonding orientation of new materials induced by rubbing treatment was described in detail through NEXAFS measurements. Both rubbed PSSA and rubbed PS indicate the same behavior for in-plane and out-of-plane asymmetries based on NEXAFS measurements. Rubbed PSSA and PS leads to an increase of number of phenyl rings with π orbitals along x than y direction and more π orbitals are preferentially tilted from the +x axis towards the z axis. PVP induced rubbing treatment shows the same behavior for in-plane asymmetry and the opposite behavior for out-of-plane asymmetry in the comparison with rubbed PSSA and PS. Generally, rubbed PS, PSSA and PVP align LC molecules perpendicular to rubbing direction, which reveal different behavior in the case of rubbed PI, PVA, and PVPD. In polystyrene family group, we can suggest that phenyl side groups determine the preferentially orientational direction of liquid crystal molecules on rubbed polymer surfaces.

The performances of rubbed PVPD are not as good and stable as those of rubbed PSSA and PVP. It can be explained by both the freedom rotation of five-sides rings in its chemical structure and weak polar anchoring energy.

Overall, among three new materials presented, the whole performances of rubbed PSSA and PVP are stable, reliable and comparable with those of rubbed PI and PVA. In conclusion, PSSA and PVP induced by rubbing treatment can be used as liquid crystal alignment materials in general and are feasible in low temperature manufacture

process for flexible substrate LCD applications in specific.

5.2 Future works

A variety of performances of different alignment materials induced by rubbing method, namely, surface morphology, the electro-optical properties of TN cells, the order parameter, the polar anchoring energy, and the in-plane and out-of-plane asymmetries of polarization-dependent NEXAFS spectra were studied in detail. However, the experimental setup of NEXAFS measurements is fixed for X-ray incident angle in this research. Hence, the measured out-of-plane asymmetry at only one certain incident angle is not enough to give a full viewpoint of the value of surface tilt angle between HSO_3 and OH groups. Consequently, to have a deeper understanding about the out-of-plane asymmetry, angular dependence of the phenyl π resonance intensity should be measured to quantify the value of the asymmetric out-of-plane surface tilt angle for new materials. Moreover, the mechanical rubbing treatment induces a pretilt angle which is known as the tilt angle of the liquid crystal with respect to the substrate surface. The pretilt angle not only prevents the formation of reverse tilted disclinations in TN LCD but also affects the LC alignment stability and the electro-optical characteristics. Furthermore, the pretilt angle is strongly affected by the surface of rubbed polymers. Therefore, the pretilt angle of these alignment materials will be investigated in detail. The relation between the surface tilt angle and the LC pretilt angle in the cells of new materials will be carried out. Besides, the relationship between the electro-optical characteristics and pretilt angle will be discussed for each material. This useful information will be very necessary in evaluating the whole performances of aligning ability as well as in explaining obviously the important role of different chemical functional groups of alignment materials.

References

- [1] D. N. L. Jiun-Haw Lee, and Shin-Tson Wu, *Introduction to Flat Panel Displays*, (2008).
- [2] M. F. Reinizer, *Chem.*, **9**, 421 (1888).
- [3] Z. P. O. Lehmann, *Chem.*, **4**, 462 (1889).
- [4] I. Dierking, *Textures of Liquid Crystals*, (1999).
- [5] I.-C. Khoo, *Liquid Crystals*, (2007).
- [6] a. S.-T. W. Deng-Ke Yang, *Fundamentals of Liquid Crystal Devices*, (2006).
- [7] J. A. R. P. J. Bos, and J. W. Doane, *Society for Info. Disp. Symp. Digest Tech.*, **24**, 887 (1993).
- [8] Y. T. Y. Tanaka, T. Sasaki, A. Takeda, Y. Koibe, and K. Okamoto, *Society for Info. Disp. Symp. Digest Tech.*, (1999).
- [9] S. M. Kelly, *Flat Panel Displays Advanced Organic Materials*, (2000).
- [10] M. Katayama, *Japan Display '89. Proc. 9th IDRC*, 6 (1989).
- [11] T. N. T. Uchida, T. Miyashita and T. Ishinaba, *Asia Display' 95. Proc. 15th IDRC*, 599 (1995).
- [12] D. K. Y. a. J. W. Doane, *SID Symp. Digest Tech. Papers*, **23**, 759 (1992).
- [13] Y. N. M. Kubo, S. Fujioka, Y. Maruyama, T. Shimada, Y. Yoshimura, M. Katayama, Y. Ishii, S. Yamakawa and A. Ban, *U.S. Patent 6295109 B1*, (2001).
- [14] P.-C. Y. a. C. Gu, *Optics of Liquid Crystal Displays*, (1999).
- [15] A. M. Vladimir Chigrinov, and Hoi Sing Kwok, *Photoalignment of Liquid Crystalline Materials: Physics and Applications*, A John Wiley & Sons (2008).
- [16] M. O. N. a. S. M. Kelly, *J. Phys. D: Appl. Phys.*, **33**, R67 (2000).
- [17] Y.-L. L. Chin-Yang Lee, Kuen Yi Wu, Ming-Yu Chen, and Jenn-Chang Hwang, *Jpn. J. Appl. Phys*, **47**, 226 (2008).
- [18] R. K. O. Yaroshchuk, A. Dobrovolsky, L. Qiu and O. D. Lavrentovich, *Liquid Crystals*, **31**, 859 (2004).
- [19] S.-S. L. a. Y.-D. Lee, *Jpn. J. Appl. Phys*, **45**, L708 (2006).
- [20] C.-Y. L. Kang-Hung Liu, Cheng-Ta Ho, Horng-Long Cheng, Shih-Ting Lin, Huang-Chin Tang, Chia-Wei Kuo, Chi-Chang Liao, Han-Ping D. Shieh, and Wei-Yang Chou, *Electrochemical and Solid-State Letters*, **10**, J132 (2007).
- [21] J. H. K.Y. Wu, C.-Y. Lee, H.-C. Tang, Y.-L. Liu, C.H. Liu, H.K. Wei, C.S. Kou, *Thin Solid Films*, **517**, 905 (2008).
- [22] K.-M. L. Byeong-Yun Oh, Byoung-Yong Kim, Young-Hwan Kim, Jin-Woo Han,

- Jeong-Min Han, Sang-Keuk Lee, and Dae-Shik Seo, *Journal of Applied Physics*, **104**, 064502 (2008).
- [23] L. S. John L. West, Kateryna Artyushkova, Jabari Farrar, Julia E. Fulghum, *SID*, 1102 (2002).
- [24] C. Mauguin, *Bull. Soc. Fr. Min.*, **34**, 71 (1911).
- [25] S.-H. Paek, *J. Ind. Eng. Chem.*, **7**, 316 (2001).
- [26] H. O. Y. B. Kim, S. Y. Park, J. W. Choi, L. Komitov, M. Matuszczyk, and S. T. Lagerwall, *Appl. Phys. Lett.*, **66**, 2218 (1995).
- [27] M. P. M. a. C. Rosenblatt, *Journal of Applied Physics*, **83**, 7649 (1998).
- [28] Y. S. a. T. U. Eung Sang Lee, *Jpn. J. Appl. Phys.*, **32**, L1822 (1993).
- [29] L. W. Yang-Ming Zhu, Zu-Hong Lu, Yu Wei, X. X. Chen and J. H. Tang, *Appl. Phys. Lett.*, **65**, 49 (1994).
- [30] D. W. Berreman, *Phys. Rev. Lett.*, **28**, 1683 (1972).
- [31] J. W. G. J. M. Geary, A. R. Kmetz, and J. S. Patel, *J. Appl. Phys.*, **62**, No. 10 (1987).
- [32] M. G. S. J. Stohr, A. Cossy-Favre, J. Diaz, Y. Momoi, S. Odahara, and T. Nagata, *Macromolecules*, **31**, 1942 (1998).
- [33] M. G. S. J. Stohr, *Journal of Electron Spectroscopy and Related Phenomena*, **98-99**, 189 (1999).
- [34] M. G. S. J. Stohr, J. Luning, A. C. Callegari, P. Chaudhari, J. P. Doyle, J. A. Lacey, S. A. Lien, S. Purushothaman, J. L. Speidell, *Science*, **292**, 2299 (2001).
- [35] K.-i. M. Dae-Shik Seo, Toh-ru Isogami, Hideaki Matsuda and Shunsuke Kobayashi, *Jpn. J. Appl. Phys.*, **31**, 2165 (1992).
- [36] H. W. Shoichi Ishihara, Keizo Nakazima, Yoshihiro Matsuo, *Liquid Crystals*, **4**, 669 (1989).
- [37] K. M. a. T. T. Shigemi Sasaki, *Jpn. J. Appl. Phys.*, **31**, L1794 (1992).
- [38] S. Lidia, *SLAC-PUB-6342*, (1993).
- [39] B. K. S. Gunther, L. Gregoratti, M. Kiskinova, *Progress in Surface Science*, **70**, 187 (2002).
- [40] J. D. A. Cossy-Favre, Y. Liu, H. R. Brown, M. G. Samant, J. Sthr, A. J. Hanna, S. Anders, and T. P. Russell, *Macromolecules*, **31**, 4957 (1998).
- [41] J. Stohr, *Springer Series in Surface Sciences*, (1992).
- [42] C. Mauguin, *Bull. Soc. Fr. Miner.*, **34**, 71 (1911).
- [43] *IBM J. Res. Dev.*, **36**, (1992).
- [44] S. W. D. a. W. E. Howard, *Sci. Am.*, **268**, 90 (1993).
- [45] K. L. M. K. W. Lee, *In Polymer Surfaces and Interfaces: Characterization, Modification and Application (VSP, The Netherlands)*, 295 (1996).
- [46] M. B. N. A. J. M. van Aerle, and R. W. J. Hollering, *J. Appl. Phys.*, **74**, 3111 (1993).
- [47] N. I. Kenji Sakamoto, Ryuichi Arafune and Sukekatsu Ushioda, *Vibrational*

- Spectroscopy*, **19**, 61 (1998).
- [48] K. I. Koichiro Shirota, Hideo Takezoe, Atsuo Fukuda and Toru Shiibashi, *Jpn. J. Appl. Phys.*, **34**, L316 (1995).
- [49] M. Deutsch, *Physical Review A*, **44**, 8264 (1991).
- [50] G. Hahner, *Chemical Society Reviews*, **35**, 1244 (2006).
- [51] Y. J. H. Chao-Huang Chen, H. F. Hsiao, S. C. Wang, W. H. Hung, D. H. Wei, and Y. L. Chan, *Proc. 8th Int. Conf. X-ray Microscopy*, 285
- [52] K. W. H. Wegner, M. Grunze, Ch. Woll, *Appl. Phys. A*, **65**, 231 (1997).
- [53] T. A. I. Mori, Hisao Ishii, Y. Ouchi, K. Seki and K. Kondo, *Journal of Electron Spectroscopy and Related Phenomena*, **78**, 371 (1996).
- [54] M. G. S. a. J. L. Joachim Stohr, *Synchrotron Radiation News*, **14**, (2001).
- [55] C. W. Klaus Weiss, Edgar Bohm, Bernd Fiebranz, Gerd Forstmann, Bin Peng, Volker Scheumann, and Diethelm Johannsmann,, *Macromolecules*, **31**, 1930 (1998).
- [56] C. W. Klaus Weiss, Diethelm Johannsmann,, *Near surface molecular orientation in polymeric alignment layers: a NEXAFS investigation*, (1999).
- [57] C. W. Klaus Weiss, Diethelm Johannsmann, *Journal of Chemical Physics*, **113**, 11297 (2000).
- [58] J. S. M. G. Samant, H. R. Brown, and T. P. Russell, *Macromolecules*, **29**, 8334 (1996).
- [59] J. S. a. D. A. Outka, *Physical Review B*, **36**, 7891 (1987).
- [60] I. M. Y. Ouchi, M. Sei, E. Ito, T. Araki, H. Ishii, K. Seki, K. Kondo, *Physica B* **208&209**, 407 (1995).
- [61] K. I. Takahiro Sakai, and Hideo Takezoe, *J. Phys. Chem. B*, **105**, 9195 (2001).
- [62] C.-H. C. Y. J. Hsu, H. F. Hsiao, W. H. Hung, D. H. Wei, Xin-Zheng Yeh and W. L. Chen,
- [63] J.-H. T. H.-M. Wu, Q. Luo, Z.-M. Zhu, Z.-H. Lu, Y. Wei, *Appl. Phys. B*, **62**, 613 (1996).
- [64] S. B. P. H. Fuoss, *Annu. Rev. Mater. Sci.*, **20**, 365 (1990).
- [65] T. P. R. Michael F. Toney, J. Anthony Logan, Hirotsugu Kikuchi, James M. Sands, and Sanat K. Kumar, *Nature*, **374**, 709 (1995).
- [66] B. J. Factor, *Macromolecules*, **26**, 2847 (1993).
- [67] <http://ssrl.slac.stanford.edu/stohr/xmcd.htm>,
- [68] C. F. Q. G. Binnig, *Phys. Rev. Lett.*, **56**, 930 (1986).
- [69] C. Polhemus, *Appl. Opt.*, **12**, 2071 (1973).
- [70] H. D. S. Filip Bruyneel, Jan Vanfleteren and Andre Van Calster, *Opt. Eng.*, **40**, 259 (2001).
- [71] S. U. a. C. R. D. F. Gu, *Liquid Crystals*, **19**, 427 (1995).
- [72] K. H. Y. a. C. Rosenblatt, *Appl. Phys. Lett.*, **43**, 62 (1983).

- [73] H. A. v. S. H. Yokoyama, *J. Appl. Phys.*, **57**, 4520 (1985).
- [74] R. D. P. Yu. A. Nastishin, S. V. Shiyonovskii, V. H. Bodnar, and O. D. Lavrentovich, *Journal of Applied Physics*, **86**, 4199 (1999).
- [75] V. C. Anatoli Murauski, Alexander Muravsky, Fion Sze-Yan Yeung, Jacob Ho, and Hoi-Sing Kwok *Physical Review E*, **71**, 061707 (2005).
- [76] <http://www.physics.ncsu.edu/stxm/polymerspectro/index.html>.
- [77] T. M. Shunsuke Kobayashi, Naoto Nishida, Yoshio Sakai, Hiroyuki Shiraki, Yukihide Shiraishi, and Naoki Toshima, *Journal of Display Technology*, **2**, 121 (2006).
- [78] N. N. Yoshio Sakai, Hiroyuki Shiraki, Yukihide Shiraishi, *Mol. Cryst. Liq. Cryst.*, **441**, 143 (2005).
- [79] X. L. Myong-Hoon Lee, Wan Kim, Seung Lee, Hyukjin Cha, *Mol. Cryst. Liq. Cryst.*, **411**, 407 (2007).
- [80] T. J. L. Suk Gyu Hahm, Seung Woo Lee, Jinhwan Yoon, and Moonhor Ree, *Materials Science and Engineering B*, **132**, 54 (2006).

